Joint Centre for Mesoscale Meteorology, Reading, UK

Parametrization of momentum transport by convection. I: Theory and Cloud modelling results

D. Gregory
R. Kershaw

Internal Report No. 54

November 1995

Met Office Joint Centre for Mesoscale Meteorology Department of Meteorology
University of Reading PO Box 243 Reading RG6 6BB United Kingdom
Tel: +44 (0)118 931 8425 Fax: +44 (0)118 931 8791
www.metoffice.com

Designed and produced by the Met Office © Crown copyright 2001 01/0240 The Met Office logo is a registered trademark.

Parametrization of momentum transport by convection. I: Theory and cloud modelling results

By R. KERSHAW and D. GREGORY
Meteorological Office, UK

To be submitted to QJRMS

SUMMARY

The theory of the mass flux approach to parametrization of convective momentum transport is presented. A cloud-resolving model is used to simulate momentum transport by ensembles of deep convective clouds in two very different regimes: a mid-latitude cold-air outbreak and tropical convection forced by convergence. Idealised, uni-directional, wind profiles are used to simplify interpretation of the results. Diagnostics relevant to the parametrization problem are presented, and it is shown that, for both regimes, the approximations inherent in the parametrization equations are reasonable. The in-cloud pressure gradients play an important role in determining the in-cloud horizontal velocities. For the cold-air outbreak case with linear shear, the results suggest that these pressure gradients are proportional to the shear and to the up/downdraught mass fluxes. Sensitivity studies suggest that the results are not very sensitive to resolution or parametrization of subgridscale processes, giving some confidence that the results are reasonably accurate. For the tropical case with the low-level jet, the pressure gradients change sign with the wind shear, and the strength depends on the organization of the convection. Both down-gradient and up-gradient momentum transports are simulated. In part II of this paper, these results are used to develop and validate a mass-flux parametrization of convective momentum transport which is tested in single column and global versions of the UK Met Office Unified Model.

1. INTRODUCTION

Over the past twenty years both modelling and observational studies have demonstrated the importance of convective momentum transports to the general circulation of the atmosphere. Houze (1973) in a study of the atmospheric angular momentum budget found that the contribution due to the vertical transport of horizontal momentum by convection was of similar magnitude to other terms. Stephens (1979) analysing GATE easterly wave data showed that significant residual existed in the observed momentum budgets of such systems which he attributed to convective activity. Early modelling studies (Helfand, 1979) suggested that convective momentum transports contribute to the intensification of the Hadley circulation while the recent study of Zhang and McFarlane (1995) has shown that such vertical transports have a large impact upon the zonal and meridional circulation as simulated by the Canadian Climate Centre model.

Several previous authors have attempted to develop parametrizations for use in large-scale models, making various assumptions regarding the evolution of the horizontal wind field within the cloud. The earliest scheme, that suggested by Schneider and Lindzen (1976), assumed that ascent would be rapid enough that in-cloud velocities could be held constant at the inflow value. However observational studies of deep convective systems (for example LeMone, 1983) have demonstrated that the cloud pressure gradients play an important role in modifying the horizontal wind inside the cloud as air ascends. More recent parametrizations (Kōnig and Ruprecht (1988), Zhang and Cho (1991a,b)) have included this effect, calculating the effect of the cloud pressure gradients from a simple model of flow around a cloud.

The momentum transports from such schemes were validated against observational estimates resulting from budget studies with varying success. However such methods do not allow details of the cloud model used in the parametrization to be well validated. For example the variation of incloud wind within the updraughts and downdraughts cannot be estimated from the observations. Neither can the important pressure gradient term. Moreover, there are few sources of observational validation, and there are large errors associated with observational estimates of momentum sources derived as residuals of a momentum budget (Stephens 1979).

This two-part paper also attempts to develop a parametrization of the vertical transport of horizontal momentum by convection. However, a different methodology is followed from that of previous studies. In this first part, a cloud resolving model is used to estimate momentum transports due to deep convection for differing flow regimes and cloud organizations. In part II, (Gregory et al 1995), these results are used to develop and validate a parametrization of convective momentum transports based upon the mass flux convection scheme of Gregory and Rowntree (1990). This is then tested in single column and global versions of the UK Met Office Unified Model. Such a methodology has several advantages over that using purely observational data. As well as estimates of the net transport of momentum the cloud resolving model simulations are able to provide details of the internal cloud structure, such as the variation of horizontal wind with height within the cloud. Also the structure and magnitude of the cloud pressure gradient can be estimated directly, without appealing to a simple cloud model, allowing representations for use in the convection scheme to be better validated.

Such an approach is consistent with that adopted by GCSS, the GEWEX Cloud Systems Study (Browning et al, 1994), with the aim of improving cloud parametrizations for large-scale models. It assumes that the current generation of cloud resolving models are able to represent correctly the main features of convective storms. This will become clearer over the next few years as projects such as the European Cloud Resolving Model project (EUCREM) undertake detailed comparison of cloud models with each other and observational data. However numerous cloud modelling studies over the past decade have already shown that such models have some skill in simulating a wide variety of cloud structures. This gives some confidence that using this data to develop a parametrization scheme for use in large-scale model is worthwhile.

2. THEORY

Consider the momentum budget of a grid square of a typical Numerical Weather Prediction (NWP) or climate model within which subgridscale convection is occurring in the presence of shear. Such a domain would cover an area ranging from, say, $(50\text{km})^2$ to $(200\text{km})^2$ or more. In order to isolate the effects of convection on momentum, we omit those terms in the momentum equation which describe the resolved large scale processes of horizontal and vertical advection, and acceleration by pressure gradients and Coriolis terms. (These terms will all be zero in our cloud model simulations.) With these assumptions, the horizontal momentum budget for the domain reduces to

$$\frac{\partial(\rho\overline{u})}{\partial t} = -\frac{\partial(\rho\overline{u'w'})}{\partial z} \tag{1}$$

where u and w are the zonal and vertical components of the wind, and ρ is the air density. A similar equation holds for the meridional component v. The overbar denotes an average over the horizontal domain and the prime denotes a departure from that average. So $\overline{u}$ is resolved by the NWP model whereas u' and w' are subgridscale (though they will be resolved by our cloud model). We make the further approximation (consistent with our cloud model) that ρ is solely

a function of height z, and define the apparent momentum source **Q3** by

$$\mathbf{Q3} = \frac{\partial \overline{\mathbf{V}}}{\partial t} = \left(-\frac{1}{\rho}\frac{\partial(\rho\overline{u'w'})}{\partial z}, -\frac{1}{\rho}\frac{\partial(\rho\overline{v'w'})}{\partial z} \right). \tag{2}$$

The problem we seek to solve is to determine **Q3**, the acceleration of the resolved flow. The problem is essentially solved once we have obtained the vertical profile of the subgridscale momentum flux.

Following the mass flux approach to cumulus parametrization (Ooyama 1971), this is achieved by partitioning the flux over the domain into contributions from convective updraughts (superscript u), convective downdraughts (superscript d), and the remainder of the domain, the 'environment' (superscript e)

$$\rho\overline{u'w'} = \sigma^u\rho\overline{u'w'}^u + \sigma^d\rho\overline{u'w'}^d + \sigma^e\rho\overline{u'w'}^e \tag{3}$$

where σ^u is the fractional area covered by convective updraughts, and σ^d and σ^e are similarly defined. The contribution from the environment is usually neglected in convective parametrization schemes (eg Gregory and Miller (1989)): we shall demonstrate later that this is reasonable using our cloud model results. The updraught contribution may be simplified by the following procedure. First replace u' by $u - \overline{u}$ so that

$$\rho\overline{u'w'}^u = \rho\overline{(u-\overline{u})w'}^u = \rho\overline{uw'}^u - \rho\overline{u}\overline{w'}^u. \tag{4}$$

Then within the updraughts we define u^* by $u^* = u - \overline{u}^u$, obtaining

$$\rho\overline{u'w'}^u = \rho\overline{(\overline{u}^u + u^*)w'}^u - \rho\overline{u}\overline{w'}^u = \rho\overline{u}^u\overline{w'}^u - \rho\overline{u}\overline{w'}^u + \rho\overline{u^*w'}^u. \tag{5}$$

We will neglect the last term $\rho\overline{u^*w'}^u$, assuming that intra-updraught correlations between u and w are small. Again, our cloud model results will justify this. Hence

$$\rho\overline{u'w'}^u = \rho(\overline{u}^u - \overline{u})\overline{w'}^u \tag{6}$$

and so we obtain the following parametrization equation for the convective momentum flux

$$\rho\overline{u'w'} = \sigma^u\rho(\overline{u}^u - \overline{u})\overline{w'}^u + \sigma^d\rho(\overline{u}^d - \overline{u})\overline{w'}^d. \tag{7}$$

This is a natural extension of the expression given by Schneider and Lindzen (1976), allowing us to consider the effects of updraughts and downdraughts separately. Thus the essence of the problem of parametrizing convective momentum flux is to predict the mass fluxes ($\rho\sigma^u\overline{w'}^u$ and $\rho\sigma^d\overline{w'}^d$) and the mean horizontal velocities in the updraughts and downdraughts.

In cumulus parametrizations, these quantities are obtained from 1-d cloud models based on the idea of entraining plumes. The mass flux is given by the vertical integration of the mass continuity equation, with horizontal convergence and divergence terms replaced by entrainment (E) and detrainment (D) rates

$$E - D = \frac{1}{\rho}\frac{\partial(\sigma^u\rho\overline{w}^u)}{\partial z}. \tag{8}$$

The vertical variation of the updraught velocity can be obtained from the momentum equation averaged over cloud updraughts, following Gregory and Miller (1989)

$$\sigma^u\overline{\frac{\partial u}{\partial t}}^u = -\sigma^u\overline{\frac{\partial u^2}{\partial x}}^u - \sigma^u\overline{\frac{\partial(uv)}{\partial y}}^u - \frac{1}{\rho}\sigma^u\overline{\frac{\partial(\rho uw)}{\partial z}}^u - \frac{1}{\rho}\sigma^u\overline{\frac{\partial p}{\partial x}}^u. \tag{9}$$

Assuming that the convection averaged over the domain is steady, so that time derivatives are zero, that the horizontal divergence terms may be approximated by entrainment and detrainment terms, and that the vertical divergence may be approximated as before, this is simplified to

$$\frac{1}{\rho}\frac{\partial(\sigma^u\rho\overline{u}^u\overline{w}^u)}{\partial z} + D\overline{u}^u - E\overline{u} = -\frac{1}{\rho}\sigma^u\overline{\frac{\partial p}{\partial x}}^u . \tag{10}$$

Equation 10 and analogous equations can be integrated to determine $\overline{u}^u$, $\overline{u}^d$, $\overline{v}^u$, and $\overline{v}^d$.

The vertical evolution of the horizontal velocity in the updraughts thus depends on the amount of entrainment and detrainment specified, and on the horizontal pressure gradient across the updraughts. The pressure gradient term is difficult to specify, far more so than the condensational heating term which replaces it in the equivalent parametrization equations for θ and q. This is what makes the parametrization of momentum transport particularly difficult.

In the remainder of this paper, we use a cloud-resolving model to evaluate the momentum transport due to convection and the quantities such as $\overline{w}^u$, $\overline{v}^u$, and $\overline{\partial p/\partial y}^u$ which are required for parametrization, as outlined above. We use idealised wind profiles (to simplify interpretation of the results) and two very different convective regimes: a mid-latitude cold-air outbreak forced by surface fluxes of heat and moisture and tropical convection forced by convergence.

3. DESCRIPTION OF CLOUD MODEL

We used the Met Office cloud-resolving model described by Shutts and Gray (1994), which solves the anelastic equations for a 3-d rectangular Cartesian grid over a flat surface. The model predicts the time variation of the three velocity components u, v, and w, pressure p, and thermodynamic variables T_l and q_t, which are conserved except when precipitation is formed:

$$T_l = T + \frac{gz}{c_p} - \frac{L_v q_l}{c_p} \tag{11}$$

$$q_t = q_v + q_l \tag{12}$$

where T is the absolute temperature, g the acceleration due to gravity, z the height above the surface, c_p the specific heat of dry air at constant pressure, L_v the latent heat of condensation of water, q_l the cloud (liquid) water mixing ratio, and q_v the water vapour mixing ratio. The model also predicts q_r, q_s, q_g, and q_i, the mixing ratios of rain, snow, graupel, and ice cloud, and N_i, the number concentration of ice crystals. The ice processes can be switched off if not required.

The domain is a box with cyclic lateral boundary conditions and no flux of air through the top or bottom. There is a no slip condition at the surface and the surface fluxes of heat and moisture are specified and held constant throughout the integration. The model has a positivity-preserving advection scheme and subgrid parametrization schemes for turbulence (1st order, stability dependent closure) and microphysics (either Kessler-type warm rain or three-phase bulk water scheme based on Lin et al (1983) and described by Swann (1994)). Although the model runs on an f-plane, $f = 0$ in these runs: rotational effects were not thought likely to be important at the horizontal scales considered here, and non-zero f complicates the model initialisation.

4. DESCRIPTION OF COLD-AIR OUTBREAK EXPERIMENTS

For the majority of the experiments, we used a domain 50km square by 15km deep, and gridlengths of 1000m horizontally and 500m vertically, though some experiments were also carried out at higher resolution to test the robustness of the results. We used horizontally uniform initial conditions, piecewise linear in height, and specified in terms of potential temperature, relative humidity, and the v-component of the wind (see Fig. 1). The other wind components u and w were initially zero, as were the microphysical variables q_l, q_r, q_s, q_g, q_i. The temperature profile was dry adiabatic to 1500m, conditionally unstable to 4km, and isothermal above the tropopause at 9km. Convection was initiated by small ($< .05$K) random temperature perturbations at each gridpoint of the lowest model level (height 250m), and maintained by the surface fluxes: $100W/m^2$ sensible heat and $400W/m^2$ latent heat. This surface moisture flux was doubled or tripled in some experiments to vary the intensity of the convection. These highly idealised initial conditions represent a mid-latitude cold air outbreak, with deep, precipitating shower clouds developing in varying unidirectional shear.

A wide range of experiments were run for two hours, to investigate the dependence of the momentum fluxes on the intensity of convection and on vertical shear. Several experiments were then extended for ten hours, for comparison with the performance of a convective parametrization in a single column model in part II (Gregory et al 1995). These extended experiments were also used for studies of the sensitivity to resolution and representation of subgridscale processes. The statistical diagnostics such as the momentum fluxes were averaged over the horizontal domain and over each hour. Most experiments were run with a damping layer above 10km, but this does not appear to have had any significant impact on the results below that level. Results from some of these experiments were reported by Kershaw (1995), but that paper concentrated on the momentum transport by waves generated above the convection. Here we focus on the transport by the convection itself.

5. COLD-AIR OUTBREAK RESULTS

(a) Preliminary tests

Table 1: LIST OF CLOUD MODEL EXPERIMENTS AND RESULTS

experiment	shear m/s/6km	latent heat flux W/m^2	ice on/off	$\sqrt{\overline{w^2}}_{max}$ m/s	$\rho\overline{vw}_{max}$ N/m^2
180	10	400	off	0.98	-0.26
181	20	400	off	0.90	-0.47
183	10	800	off	1.30	-0.33
184	20	800	off	1.21	-0.67
185	30	800	off	1.19	-1.05
160	10	1200	off	1.58	-0.42
164	20	1200	off	1.47	-0.86
169	30	1200	off	1.40	-1.23
170	40	1200	off	1.43	-1.88

The first set of experiments are listed in Table 1, which also gives some statistical diagnostics from the second hour of each experiment. To help explain these diagnostics we present some results from the control simulation [180]. Figure 2 shows the simulated vertical velocity field in the middle of the convective layer after 2 hours. We see an ensemble of updraughts, the

strongest having a peak velocity of more than 8m/s, surrounded by much weaker descending motion. The strongest downdraughts (-2m/s) at this level are in the ring of compensating subsidence which surrounds the most active updraughts. Figure 3 shows the perturbation, the difference from the mean, in the v-component of the wind at the same level, for comparison with the vertical velocities. The updraughts tend to be associated with negative v', implying negative momentum fluxes. At the lowest model level, the vertical velocity field (not shown) is much less skewed, indeed the peak downdraughts (driven by precipitation) are slightly stronger (-2.7m/s) than the peak updraughts (2.5m/s). Positive (negative) perturbations in the v-component (not shown) at the same level tend to occur downstream (upstream) of the downdraughts, as these spread out on approaching the surface. There is no very clear indication of the likely sign of the momentum flux at this level, though we will see later that the downdraughts tend to act to oppose the updraughts: they have positive momentum flux. Figure 4 shows the vertical profile of the standard deviation of w over the domain, which provides one measure of the intensity of convective activity in the model. We use the peak value of this diagnostic ($\sqrt{\overline{w^2}}_{max}$), marked with a star in the figure, to compare the convective intensity in the different experiments. Figure 5 shows the vertical profile of the momentum flux, which is negative except at the lowest model level and has maximum magnitude in the middle of the convective layer. The convection (in all the cold-air outbreak experiments) is transporting momentum down gradient and so acting to reduce the vertical shear. We use the peak value ($\rho\overline{vw}_{max}$), marked with a star, to compare the convective momentum transport in the experiments.

The diagnostics in Table 1 show that increasing the surface flux of latent heat increases the intensity of convection and the convective momentum flux. Increasing the shear tends, in general, to decrease the convective intensity slightly, but increase the momentum flux. This result is summarised in Figure 6, which shows that there is an approximately linear relationship between convective momentum flux and the product of the shear (ΔV) and the convective intensity ($\sqrt{\overline{w^2}}_{max}$). The simplicity of this relationship is encouraging because it suggests that successful parametrization of the process of convective momentum transport is possible, at least when the convection is not organized on the mesoscale. The linearity of the relationship also suggests that it is only necessary to compare the parametrization with a subset of the experiments listed in Table 1.

(b) Simulations for comparison with single column model

Table 2 shows details of the experiments which were run for comparison with the single column model [232,233,236,237]. The new control experiment [232] is identical to experiment [180], save that it includes the microphysical parametrization of ice processes which became available during the course of this research. The other three experiments were chosen in order to validate the parametrization in part II (Gregory et al 1995) over a range of shear and with differing intensity of convective activity.

The cloud model simulations are not just useful because they provide an estimate of the net effect of convection on the wind profile **Q3**, they also enable us to diagnose those quantities which are intrinsic to the parametrization equation 7 and to test some of the underlying assumptions made in deriving and applying it. Figure 7, for example, shows the updraught and downdraught mass fluxes averaged over the ten hours of two of the simulations. (For the purpose of calculating partitioned diagnostics such as these, an updraught is occurring at a gridpoint if the vertical velocity is greater than +1m/s and the total condensed water content exceeds 0.1g/kg. A downdraught is indicated by negative vertical velocity and precipitating water content exceeding 0.1g/kg.) Note that the updraught fluxes ($\rho\sigma^u\overline{w}^u$) peak at 2km, implying net detrainment above this level. The downdraught fluxes ($\rho\sigma^d\overline{w}^d$) peak at the lowest model level, achieving 60-70%

Table 2: LIST OF COMPARISON EXPERIMENTS

experiment	shear m/s/6km	latent heat flux W/m^2	ice on/off	Δx m	Δz m	l m
232	10	400	on	1000	500	230
233	20	400	on	1000	500	230
236	10	800	on	1000	500	230
237	20	800	on	1000	500	230
242	20	800	on	500	500	115
246	20	800	off	1000	500	230
247	20	800	off	1000	500	150
248	20	800	off	1000	100-700	230

of the updraught magnitude and implying net entrainment over most of their depth. All four experiments show this same structure. The mass fluxes are almost identical in those pairs of experiments in which only the vertical shear was changed: [232,233] and [236,237]. Hence, for clarity, only mass fluxes for [232] and [236] are included in the figure. Comparison of these two experiments shows the effect of doubling the surface moisture flux: the peak updraught mass flux is increased by about 70% and deepened; the downdraught flux is also increased.

Using the model, the pressure gradient forces across the updraughts and downdraughts may be diagnosed directly. Fig. 8 shows that parcels of air in the updraughts must be accelerated by pressure gradients across the cloud as they ascend. Similarly, except at the lowest model level, the downdraughts are decelerated by pressure gradients as they descend. This is confirmed by Fig. 9, which shows the horizontal velocity in the draughts (up or down) and the domain average. Note that the difference $\overline{v}^u - \overline{v}$ is always negative, implying negative momentum transport, and the difference $\overline{v}^d - \overline{v}$ is also negative, implying positive momentum transport. Thus the downdraughts are mainly composed of air which has previously ascended in an updraught. If they were transporting (anomalously) high momentum air downwards we would expect this difference to be positive, which would imply negative momentum flux. That this is not the case is confirmed by Fig. 10; the downdraught momentum flux is of opposite sign to the updraught flux. This is true of all four experiments, but it will not always be so; it will depend on the structure of the convection. An example of co-operative updraught-downdraught transport will be presented in Section 7. Note that the updraught transports are by far the most important; they account for nearly all the total transport. Again, this is true in all four experiments. Figure 10 also shows a comparison of the updraught and downdraught momentum transports with the estimates of those quantities obtained from parametrization equation 7, the product of the mass flux and the velocity anomaly. The agreement is very good, indicating that the terms neglected in equation 7 are not important. This is so in all four experiments.

Figure 11 shows the net effect of convection (and subgridscale turbulence) on the v-component of the wind (effectively **Q3**) in all four experiments. The down-gradient transports have eroded the shear in the middle of the convective layer, accelerating the flow below 4km and decelerating it above. **Q3** is enhanced by shear and by increased convective activity. Increasing the shear (in [233]cf[232] and [237]cf[236]) increases the momentum transport by increasing $\overline{v}^u - \overline{v}$. (Remember that the mass flux is largely unchanged by increased shear.) Increasing the mass flux (in [236]cf[232] and [237]cf[233]) actually decreases $\overline{v}^u - \overline{v}$ slightly, so the effect on **Q3** is not quite proportional to the mass flux. The pressure gradient force across the updraught increases with shear and with updraught mass flux. This will be presented and discussed in part II.

(c) Sensitivity tests

Table 2 also shows details of the sensitivity tests which were carried out to aid assessment of the accuracy of the cloud-model results: [242] cf [237] shows the effect of increasing horizontal resolution; [248] cf [246] shows the effect of increasing vertical resolution in the boundary layer; [247] cf [246] shows the sensitivity to turbulence parametrization; [237] cf [246] shows the effect of including a representation of the ice phase. Most of these changes are self-explanatory, however the change in turbulence parametrization requires some explanation. The parameter l is a mixing length which is usually related to the horizontal gridlength in our simulations by the relationship $l = c_s \Delta x$ where $c_s = 0.23$. Thus in the simulation with double the horizontal resolution [242] l is halved. In simulation [247] a smaller value $c_s = 0.15$ is used. As the eddy viscosity is proportional to l^2 this has the effect of reducing the turbulent (subgridscale) fluxes of heat moisture and momentum, and increasing the resolved fluxes. Using a much smaller value than $c_s = 0.15$ would be likely to lead to noisy simulations, whereas using a much larger value than $c_s = 0.23$ would result in excessively smooth simulations. We have thus tested the sensitivity to the acceptable range of values of c_s. Further details of the turbulence parametrization are given in Shutts and Gray (1994) (where l is called λ_0) and a comparison with parametrizations in other Large Eddy Simulation codes may be found in Andren et al (1994).

The results of the sensitivity tests are summarised in Fig. 12. They show that the momentum transport in the simulations is not very sensitive to any of these details, giving us confidence that our estimates of **Q3** for these experiments are accurate to, say, $\pm 10\%$.

Although the net momentum transport is insensitive to these changes, some aspects of the simulations are sensitive to the details of the model, however. In particular, cloud amounts in the upper troposphere are doubled when the ice phase is included, and ice processes (presumably melting) enhance the downdraught mass flux by 40%. Increasing the horizontal resolution does have some impact on the momentum transports because the updraughts are better resolved. Hence the pressure gradient force across the updraughts is stronger, producing a smaller updraught-environment velocity difference $(\overline{v}^u - \overline{v})$. Thus there is slightly less momentum transport in the model at higher resolution even though the mass fluxes are greater.

6. DESCRIPTION OF TROPICAL EXPERIMENTS

Table 3: TROPICAL EXPERIMENTS

experiment	2d/3d	domain size km	ice on/off	Δx m	Δy m	Δz m
234	2d	500*20	on	-	1000	500
235	3d	50*50*20	on	1000	1000	500

We next present results for a case study in which the convective regime is quite different. Whereas the cold-air outbreak case is for a very unstable airstream in which convection is strongly forced by surface fluxes, we choose a tropical case with only weak surface fluxes in which the convection is forced by large scale convergence. The initial profiles are shown in Fig. 13. The temperature and moisture are based on the 20 hour profiles from the composite GATE easterly wave dataset (Thompson et al 1979), as used by Gregory and Miller (1989). The initial v is again an idealised profile. It is chosen because such a low level jet is a favorable

environment for formation of tropical squall lines. We ran two experiments, detailed in Table 3, which differed only in that they had different horizontal domains, one 3-dimensional, simulating random tropical convection, the other 2-dimensional, simulating squall line organization.

As in the cold-air outbreak experiments, the other wind components u and w were initially zero, as were the microphysical variables q_l, q_r, q_s, q_g, q_i. Convection was again initiated by small ($< .05$K) random temperature perturbations at each gridpoint of the lowest model level (height 250m), but the surface fluxes were much weaker: $10W/m^2$ sensible heat and $125W/m^2$ latent heat. The convection was driven by imposed cooling and moistening due to domain scale ascent. The forcing rates were as shown in Fig. 14, smoothed versions of those used in Gregory and Miller (1989). They were applied throughout the 10 hours of each experiment, uniformly over the horizontal domain.

7. TROPICAL RESULTS

(a) 3-d simulation

The convective mass fluxes averaged over the 10 hours of experiment [235] are shown in Fig. 15. Note that although they are weaker than those in the cold-air outbreak simulations, they share the same structure. The peak updraught mass flux is near cloud base, implying net detrainment at all levels above. For the GATE case, there is observational evidence to support this result. Thompson et al (1979) reported a maximum in the average vertical (pressure) velocity at around 800hPa (2km) during phase III of the experiment and deduced from the associated vertical profile of horizontal divergence that convective clouds tended to have tops near 800hPa, 500hPa (5km) and 250hPa (10km). More recently, Cheng (1989) calculated updraught and downdraught mass fluxes diagnosed from phase III-mean data; these have the same structure as our modelled mass fluxes. Previous work by Yanai et al (1976), on Marshall Islands data, by Nitta (1975), on data from BOMEX, and by Soong and Tao (1984), on a particular rainband during GATE, also showed updraught mass fluxes which decreased with height. Using profiles similar to those used here, Gregory and Miller (1989) also found that updraught mass flux decreased above 700mb, implying a deep layer of detrainment. The magnitude of their simulated mass flux was similar to that reported here.

The in-cloud pressure gradients are shown in Fig. 16. Note that the sign seems to depend on the sign of the wind shear, and that the force across the downdraught opposes the force across the updraught at each level. The convective momentum fluxes are shown in Fig. 17. As in the cold-air outbreak, the updraughts account for most of the momentum transport and the downdraughts act in the opposite sense to the updraughts. The convection is transporting momentum down gradient, away from the jet, because updraughts contain air of anomalously low v below jet level and anomalously high v above the jet. The pressure gradient forces are acting, as in the cold air outbreak case, to maintain $\overline{v}^u$ close to $\overline{v}$, thus moderating the convective momentum transport. Figure 17 also shows the estimates of the momentum transports obtained from parametrization equation 7, the product of the mass flux and the velocity anomaly. The agreement is very good for the updraught component, though less good for the downdraught. As the downdraught term is not important, we conclude that in this experiment too the terms neglected in equation 7 are not important. The net effect of the convection (Fig. 18) is to weaken the jet and to accelerate the flow near the surface and above 6km.

(b) 2-d simulation

The 2-d simulation was made to investigate the effect of a common form of organization of tropical convection, the squall line, on the convective momentum transport, and to give guidance on parametrization. Observational evidence (LeMone 1983, LeMone et al 1984) suggests that whereas line-parallel momentum transport by tropical rainbands is down gradient, weakening the shear as in our 3-d simulations (tropical and mid-latitude), line-normal momentum transport is up gradient, strengthening the shear.

The convective mass fluxes averaged over the 10 hours of the 2d experiment [234] are shown in Fig. 15. Note that they are very similar to those from the 3d experiment, though the downdraughts are somewhat stronger. The in-cloud pressure gradients are shown in Fig. 19. Note that the sign again depends on the sign of the wind shear, and again the force across the downdraught opposes the force across the updraught at each level. The magnitude of the force is about 5 times larger though in the 2d simulation than in the 3d simulation, producing quite different momentum transports. The convective momentum fluxes are shown in Fig. 20. In this simulation updraughts and downdraughts act in the same sense, and the total flux is negative at all levels. In particular it is up gradient above the jet. Figure 20 also shows the estimates of the momentum transports obtained from parametrization equation 7. The agreement is very good for both components, confirming that in this experiment too equation 7 is a good approximation. The net effect (Fig. 18) is to maintain the strength of the jet and to decelerate the flow (producing negative v) above 6km, thus maintaining and deepening the shear layer at mid levels rather than weakening it as in the 3d simulation. This is achieved by an organization of the convection into squall lines, one of which is shown in Fig. 21. Note that the updraught tilts backwards (left) with height, relative to the direction of propagation (right), and consists of air with negative v'. This front-to-rear flow is strengthened by the pressure gradient force acting across the updraught in the negative y-direction. Unlike in the 3-d experiments, the downdraught originates as a distinct rear-to-front flow at $\sim$ 3km and consists of air with positive v'. It is thus able to reinforce the updraught momentum transport rather than oppose it, as in observed squall lines (eg LeMone 1983).

8. CONCLUSIONS

We have used a cloud-resolving model to simulate momentum transport by ensembles of deep convective clouds in two very different regimes: a mid-latitude cold-air outbreak forced by surface fluxes of heat and moisture, and tropical convection forced by convergence. We used idealised, uni-directional, wind profiles to simplify interpretation of the results. (The inclusion of directional shear would be a natural extension of this work.) We have shown that, for the cold-air outbreak, the momentum transport is, to a good approximation, proportional to the product of the shear and the convective intensity, and that, for the two regimes studied here, the approximations inherent in parametrization equation 7 are reasonable. Also, it is clear that the in-cloud pressure gradients play an important role in determining the in-cloud horizontal velocities, confirming previous studies. For the cold-air outbreak case with linear shear, our results suggest that these pressure gradients are proportional to the shear and to the up/downdraught mass fluxes. For the tropical case with the low-level jet, the pressure gradients change sign with the wind shear, and the strength depends on the organization of the convection. In the 3-d simulation, where the convection appears to be randomly organized, and consists of relatively shortlived storms, the momentum is transported down gradient. In the 2-d simulation, the convection has the structure of longer-lived squall lines and the momentum transport is up gradient, organized by much stronger pressure gradients.

In a companion paper (Gregory et al 1995), these results are used to develop and validate a mass-flux parametrization of convective momentum transport which is tested in single column

and global versions of the UK Met Office Unified Model. There is of course an inherent danger in using a cloud model to provide validation data. However, sensitivity studies suggest that the results presented here are not very sensitive to resolution or parametrization of subgridscale processes, giving us some confidence that the results are reasonably accurate.

REFERENCES

Andren, A., Brown, A. R., Graf, J., Mason, P. J., Moeng, C.-H., Nieuwstadt, F. T. M. and Schumann, U. (1994) Large-eddy simulation of a neutrally stratified boundary layer: A comparison of four computer codes. *Q. J. R. Meteorol. Soc.*, **120**, 1457–1484

Browning, K. A. et al (1994) GEWEX Cloud System Study (GCSS): science plan. World Climate Research Programme. International GEWEX Project Office. *IGPO Publication Series* No. **11**

Cheng, M.-D. (1989) Effects of downdrafts and mesoscale convective organization on the heat and moisture budgets of tropical cloud clusters. Part II: Effects of convective-scale downdrafts. *J. Atmos. Sci.*, **46**, 1540–1564

Gregory, D., Kershaw, R. and Inness, P. M. (1995) Parametrization of momentum transport by convection. II: Tests in single column and general circulation models. Submitted to Q. J. R. Meteorol. Soc.

Gregory, D. and Miller, M. J. (1989) A numerical study of the parametrization of deep tropical convection. *Q. J. R. Meteorol. Soc.*, **115**, 1209–1241

Gregory, D. and Rowntree, P. R. (1990) A mass flux convection scheme with representation of cloud ensemble characteristics and stability-dependent closure. *Mon. Wea. Rev.*, **118**, 1483–1506

Helfand, H. M. (1979) The effect of cumulus friction on the simulation of the January Hadley circulation by the GLAS model of the general circulation. *J. Atmos. Sci.*, **36**, 1827–1843

Houze, R. A., Jr. (1973) A climatological study of vertical transport by precipitating cumuli. *J. Atmos. Sci.*, **30**, 1112–1123

Kershaw, R. (1995) Parametrization of momentum transport by convectively generated gravity waves. *Q. J. R. Meteorol. Soc.*, **121**, 1023–1040

Kõnig, W. and Ruprecht, E. (1988) Effects of convective clouds on the large-scale vorticity budget. *Meteorol. and Atmos. Phys.*, **41**, 213–229

LeMone, M. A. (1983) Momentum transport by a line of cumulonimbus. *J. Atmos. Sci.*, **40**, 1815–1834

LeMone, M. A., Barnes, G. M. and Zipser, E. J. (1984) Momentum flux by lines of cumulonimbus over the tropical oceans. *J. Atmos. Sci.*, **41**, 1914–1932

Lin, Y.-L., Farley, R. D. and Orville, H. D. (1983) Bulk parametrization of the snow field in a cloud model. *J. Clim. Appl. Meteorol.*, **22**, 1065–1092

Nitta, T. (1975) Observational determination of cloud mass flux distributions. *J. Atmos. Sci.*, **32**, 73–91

Ooyama, K. (1971) A theory on parametrization of cumulus convection. *J. Meteorol. Soc. Japan*, **49**, 744–756

Schneider, E. K. and Lindzen, R. S. (1976) A discussion of the parametrization of momentum exchange by cumulus convection. *J. Geophys. Res.*, **81**, 3158–3160

Shutts, G. J. and Gray, M. E. B. (1994) A numerical modelling study of the geostrophic adjustment process following deep convection. *Q. J. R. Meteorol. Soc.*, **120**, 1145–1178

Soong, S.-T. and Tao, W.-K. (1984) A numerical study of the vertical transport of momentum in a tropical rainband. *J. Atmos. Sci.*, **41**, 1049–1061

Stephens D. (1979) Vorticity, momentum and divergence budgets of synoptic-scale wave disturbances in the tropical eastern Atlantic. *Mon. Wea. Rev.*, **107**, 535–550

Swann, H. A. (1994) Cloud microphysical processes — a description of the parametrization used in the Large Eddy Model. Joint Centre for Mesoscale Meteorology Internal Report No. 10. Available from JCMM, Reading University.

Thompson, R. M., Payne, S. W., Recker, E. E. and Reed, R. J. (1979) Structure and properties of synoptic-scale wave disturbances in the intertropical convergence zone of the eastern Atlantic. *J. Atmos. Sci.*, **36**, 53–72

Yanai, M., Chu, J.-H., Stark, T. E. and Nitta, T. (1976) Response of deep and shallow tropical maritime cumuli to large-scale processes. *J. Atmos. Sci.*, **33**, 976–991

Zhang,G. J. and Cho, H.-R. (1991a) Parametrization of the vertical transport of momentum by cumulus clouds. Part I: theory. *J. Atmos. Sci.*, **48**, 1483–1492

Zhang,G. J. and Cho, H.-R. (1991b) Parametrization of the vertical transport of momentum by cumulus clouds. Part II: application. *J. Atmos. Sci.*, **48**, 2448–2457

Zhang,G. J. and McFarlane, N.A. (1995) Role of convective scale momentum transport in climate simulation. *J. Geophys. Res.*, **100**, 1417–1426

FIGURE CAPTIONS

Fig. 1 Initial profiles of (a) θ (solid) and θ_e (stars), (b) q_t (solid) and q_{sat} (crosses), and (c) v in cold-air outbreak experiments. See Tables 1 and 2 for details.

Fig. 2 Horizontal section through control simulation [180] showing vertical velocity at 4km, after 2 hours. Contour interval: 1m/s, dashed contours negative.

Fig. 3 Horizontal section through control simulation [180] showing v' at 4km, after 2 hours. Contour interval: 1m/s, dashed contours negative.

Fig. 4 Vertical profile of rms vertical velocity averaged over second hour of control simulation [180].

Fig. 5 Vertical profile of momentum flux averaged over second hour of control simulation [180].

Fig. 6 Scatter plot of momentum flux plotted against product of shear and rms w, averaged over second hour of the numerical experiments.

Fig. 7 Vertical profile of partitioned mass fluxes averaged over ten hours of simulations [232] (stars: updraught; diamonds: downdraught) and [236] (squares: updraught; plus signs: downdraught).

Fig. 8 Vertical profile of acceleration due to horizontal pressure gradient averaged over ten hours of control simulation [232] (stars: updraught; diamonds: downdraught).

Fig. 9 Vertical profile of partitioned velocities averaged over ten hours of control simulation [232] (solid line: domain average; stars: updraught; diamonds: downdraught).

Fig. 10 Vertical profile of partitioned momentum fluxes averaged over ten hours of control simulation [232] (solid line: domain average; stars: updraught; diamonds: downdraught) plus estimates based on equation 7 (dashed: updraught estimate; dash-dotted: downdraught estimate).

Fig. 11 Change in $\overline{v}$ over ten hours of simulation (plus signs: [232], stars: [233], diamonds: [236], crosses: [237]).

Fig. 12 Change in $\overline{v}$ over ten hours of simulation (plus signs: [237], stars: [242], diamonds: [246], triangles: [247], crosses: [248]).

Fig. 13 Initial profiles of (a) θ (solid) and θ_e (stars), (b) q_t (solid) and q_{sat} (crosses), and (c) v in tropical experiments.

Fig. 14 Forcing profiles for temperature (solid), and moisture (dashed) in tropical experiments.

Fig. 15 Vertical profile of partitioned mass fluxes averaged over ten hours of simulations [235] (stars: updraught; diamonds: downdraught) and [234] (plus signs: updraught; triangles: downdraught).

Fig. 16 Vertical profile of acceleration due to horizontal pressure gradient averaged over ten hours of simulation [235] (stars: updraught; diamonds: downdraught).

Fig. 17 Vertical profile of partitioned momentum fluxes averaged over ten hours of simulation [235] (solid line: domain average; stars: updraught; diamonds: downdraught) plus estimates based on equation 7 (dashed: updraught estimate; dash-dotted: downdraught estimate).

Fig. 18 $\overline{v}$ initially (solid), after ten hours of 3-D simulation [235] (dashed), and after ten hours of 2-D simulation [234] (dotted).

Fig. 19 Vertical profile of acceleration due to horizontal pressure gradient averaged over ten hours of simulation [234] (plus signs: updraught; triangles: downdraught).

Fig. 20 Vertical profile of partitioned momentum fluxes averaged over ten hours of simulation [234] (solid line: domain average; plus signs: updraught; triangles: downdraught) plus estimates based on equation 7 (dashed: updraught estimate; dash-dotted: downdraught estimate).

Fig. 21 Vertical section showing wind vectors in part of domain of simulation [234] after 6 hours. The horizontal mean has been subtracted from the v-component.

Fig. 1 Initial profiles of (a) θ (solid) and θ_e (stars), (b) q_t (solid) and q_{sat} (crosses), and (c) v in cold-air outbreak experiments. See Tables 1 and 2 for details.

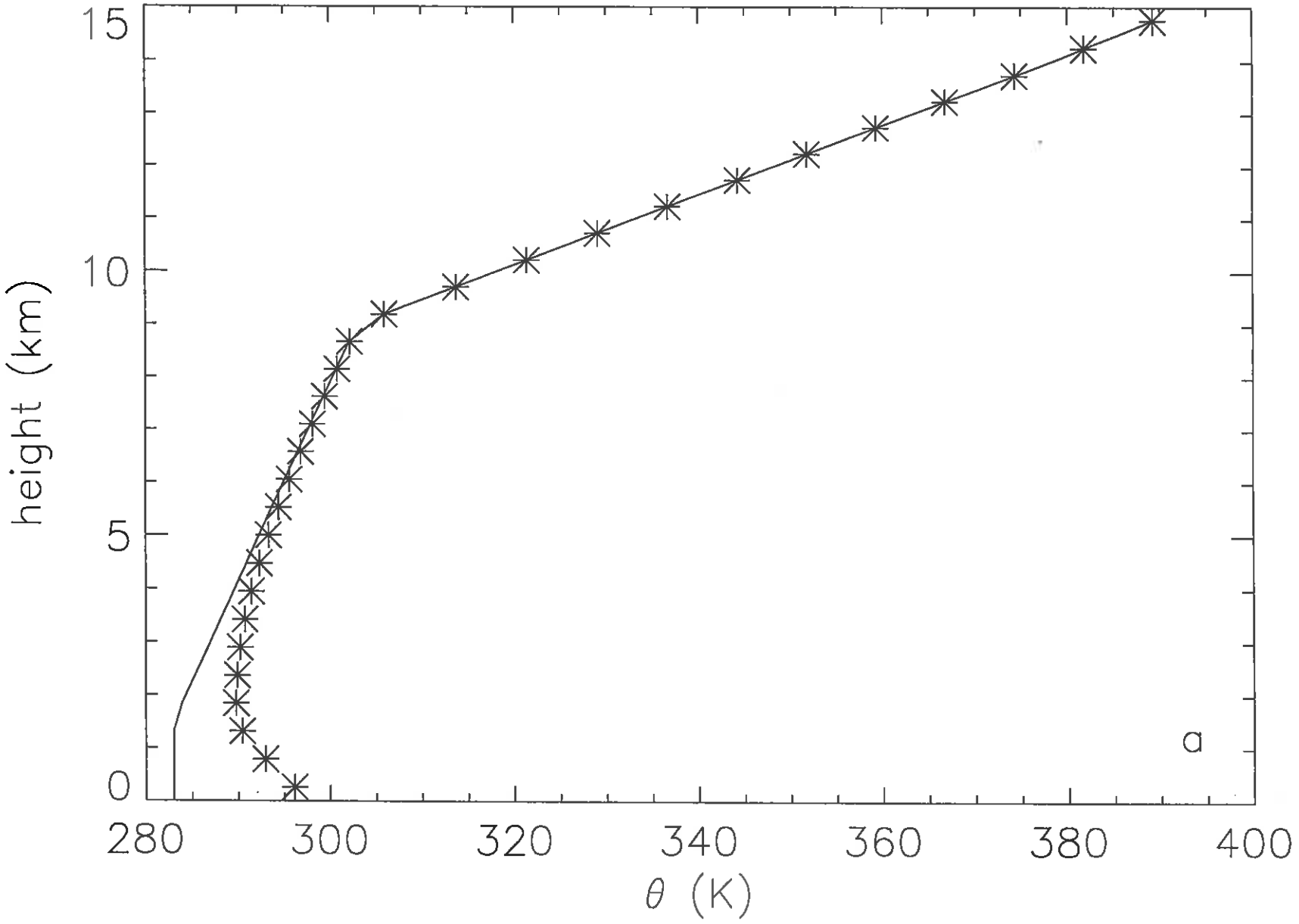

27/10/1995 15:37:45.000

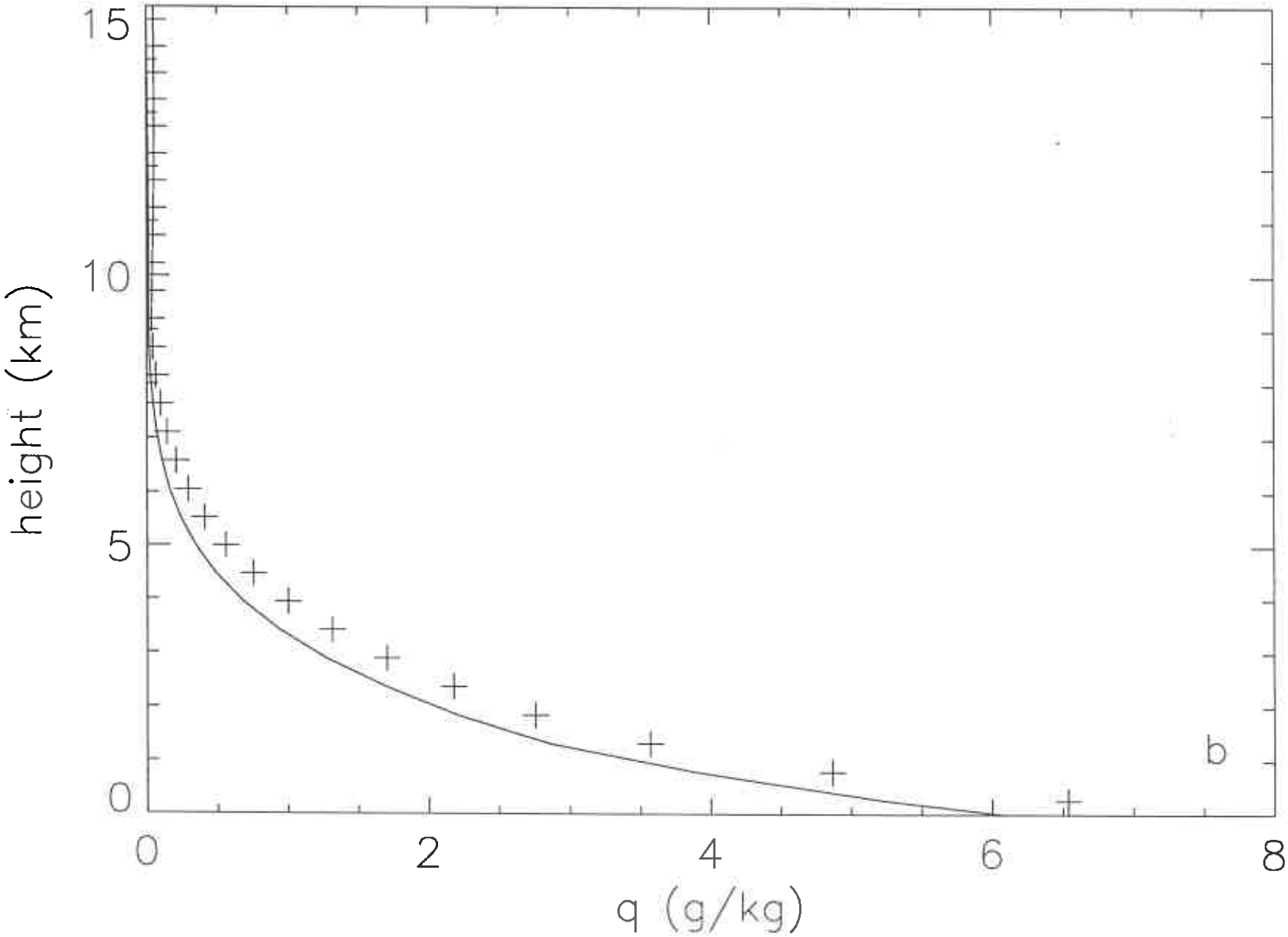

27/10/1995 15:51:01.000

Fig. 2 Horizontal section through control simulation [180] showing vertical velocity at 4km, after 2 hours. Contour interval: 1m/s, dashed contours negative.

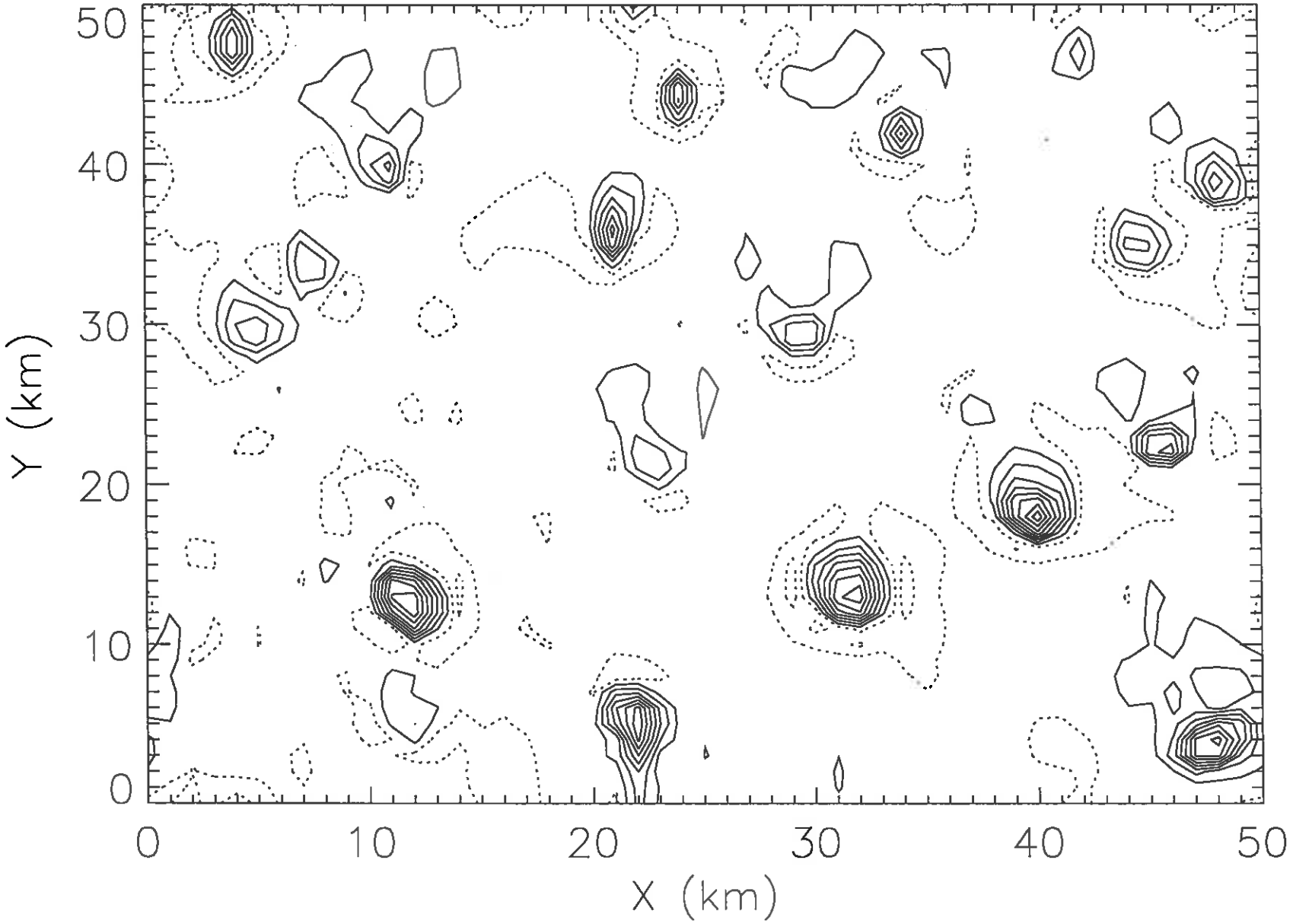

03/11/1995 14:32:21.000

Fig. 2 Horizontal section through control simulation [180] showing vertical velocity at 4km, after 2 hours. Contour interval: 1m/s, dashed contours negative.

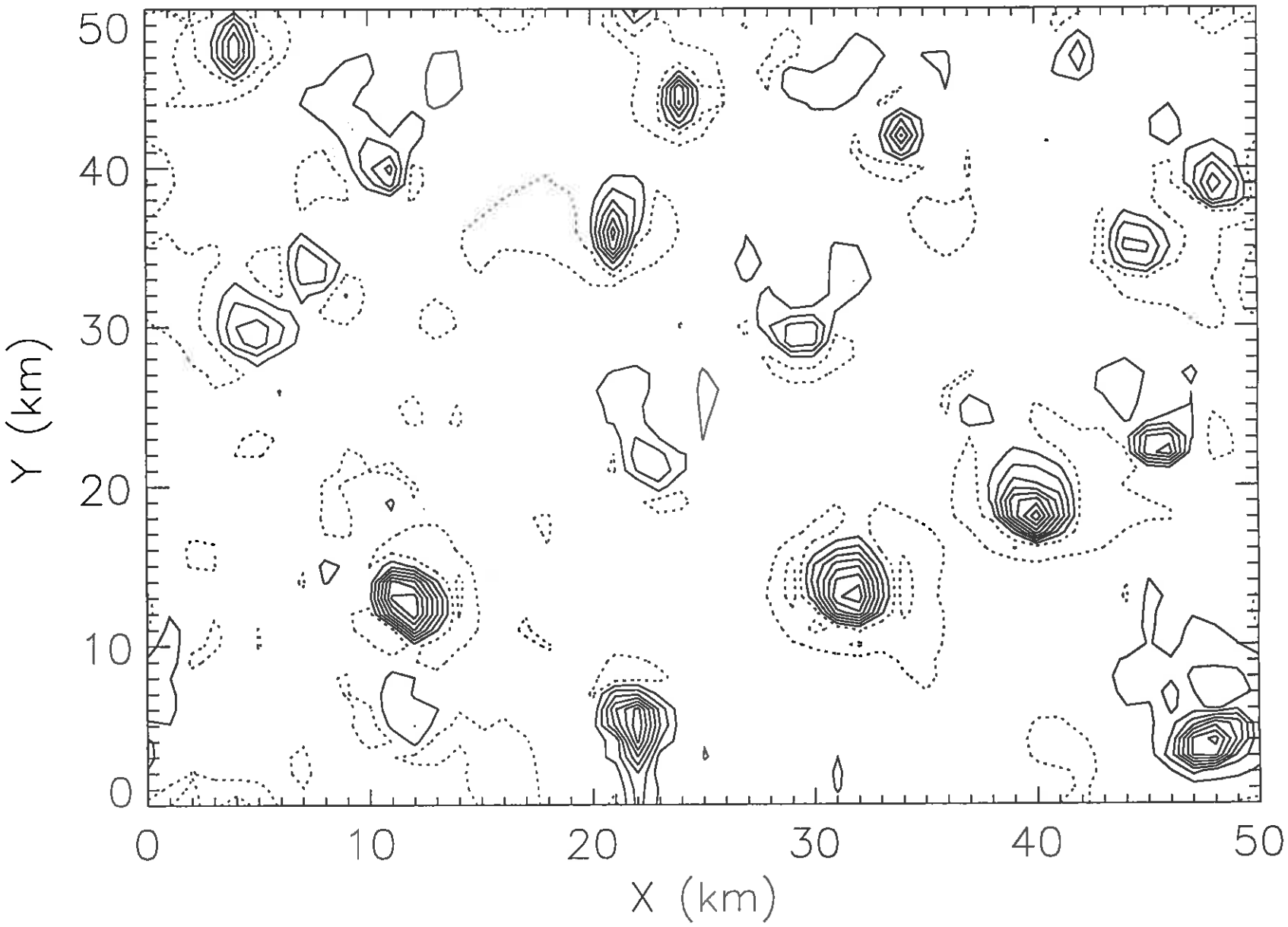

03/11/1995 14:32:21.000

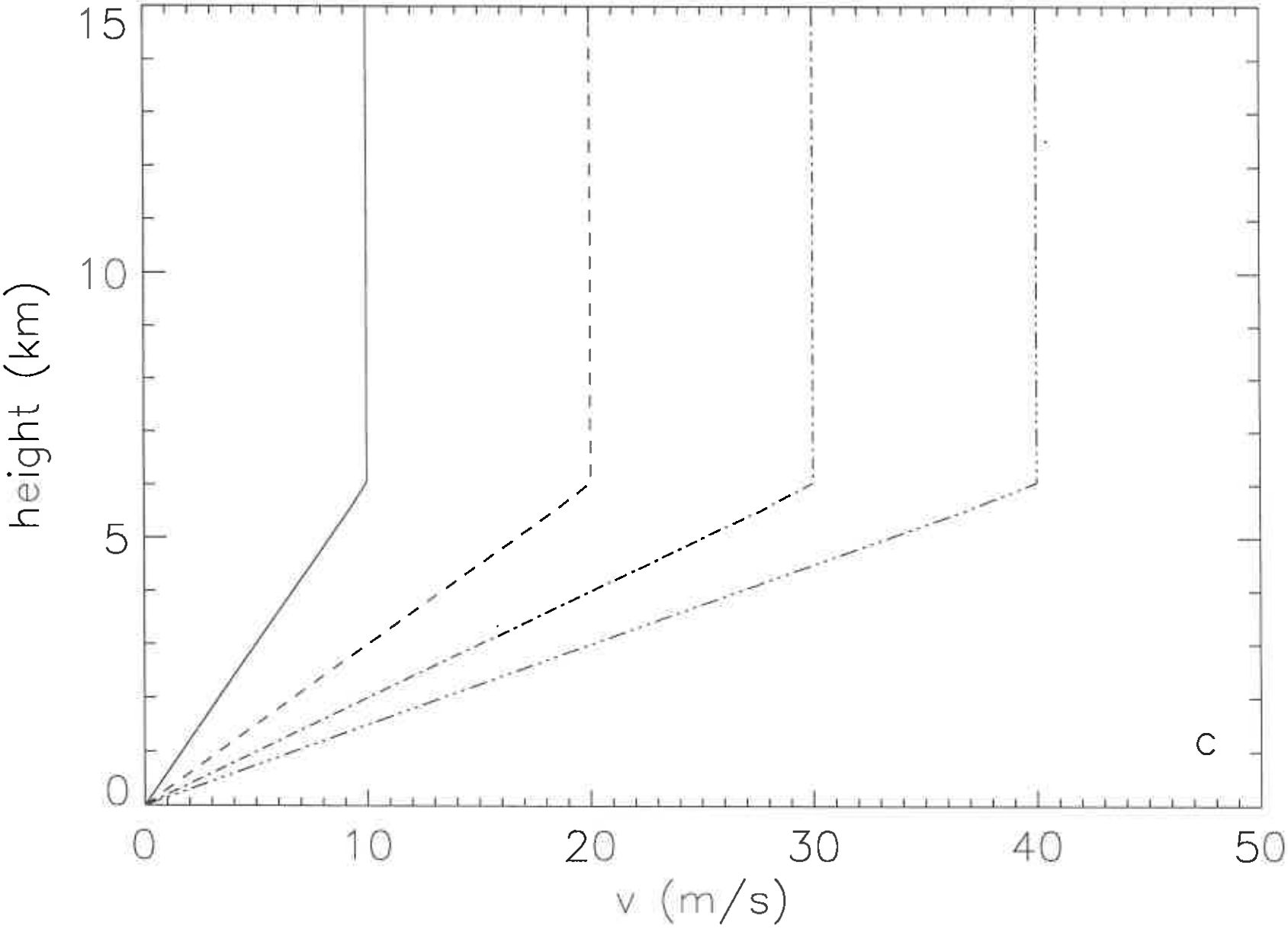

27/10/1995 16:09:01.000

Fig. 3 Horizontal section through control simulation [180] showing v' at 4km, after 2 hours. Contour interval: 1m/s, dashed contours negative.

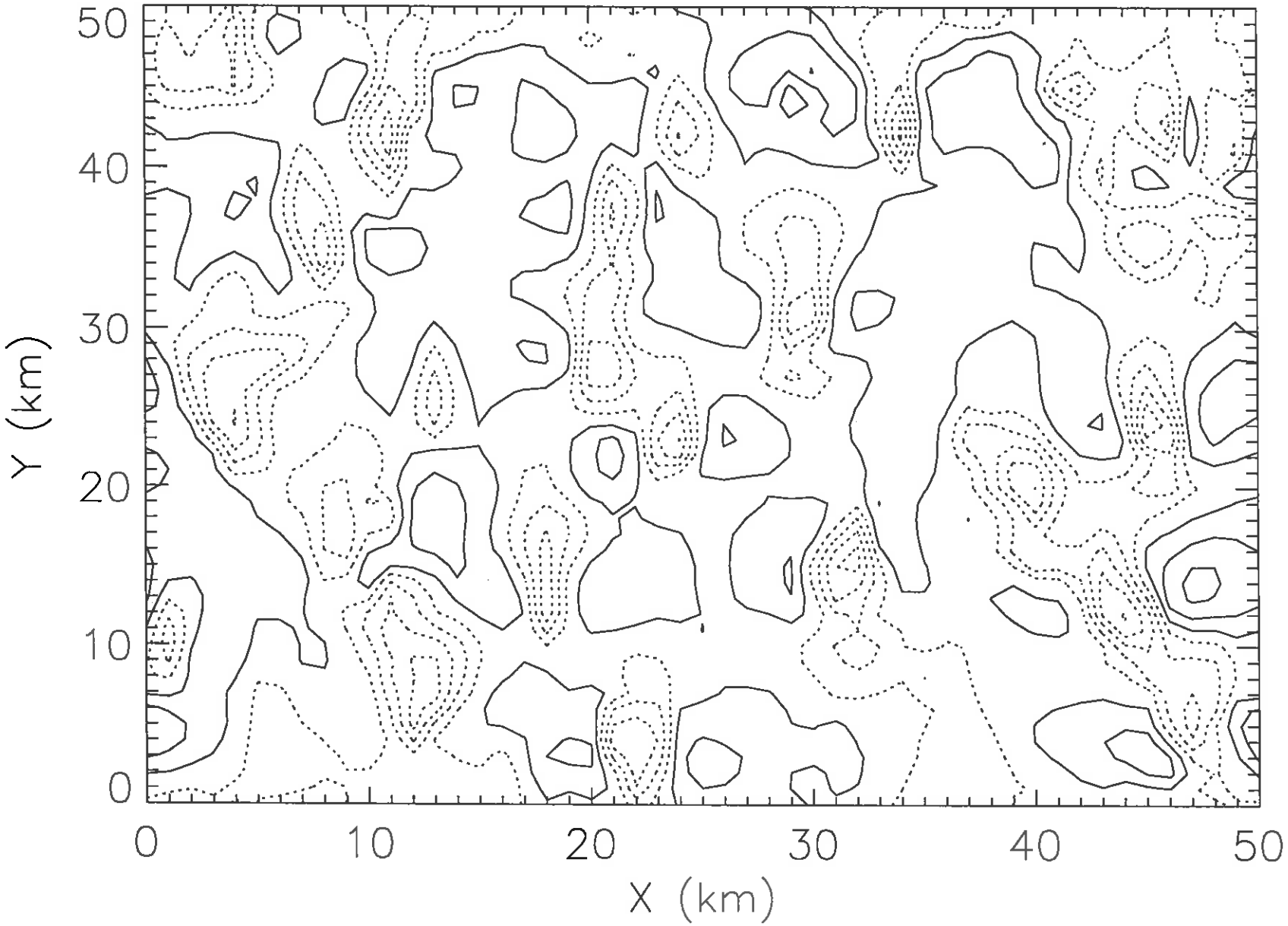

03/11/1995 14:31:16.000

Fig. 4 Vertical profile of rms vertical velocity averaged over second hour of control simulation [180].

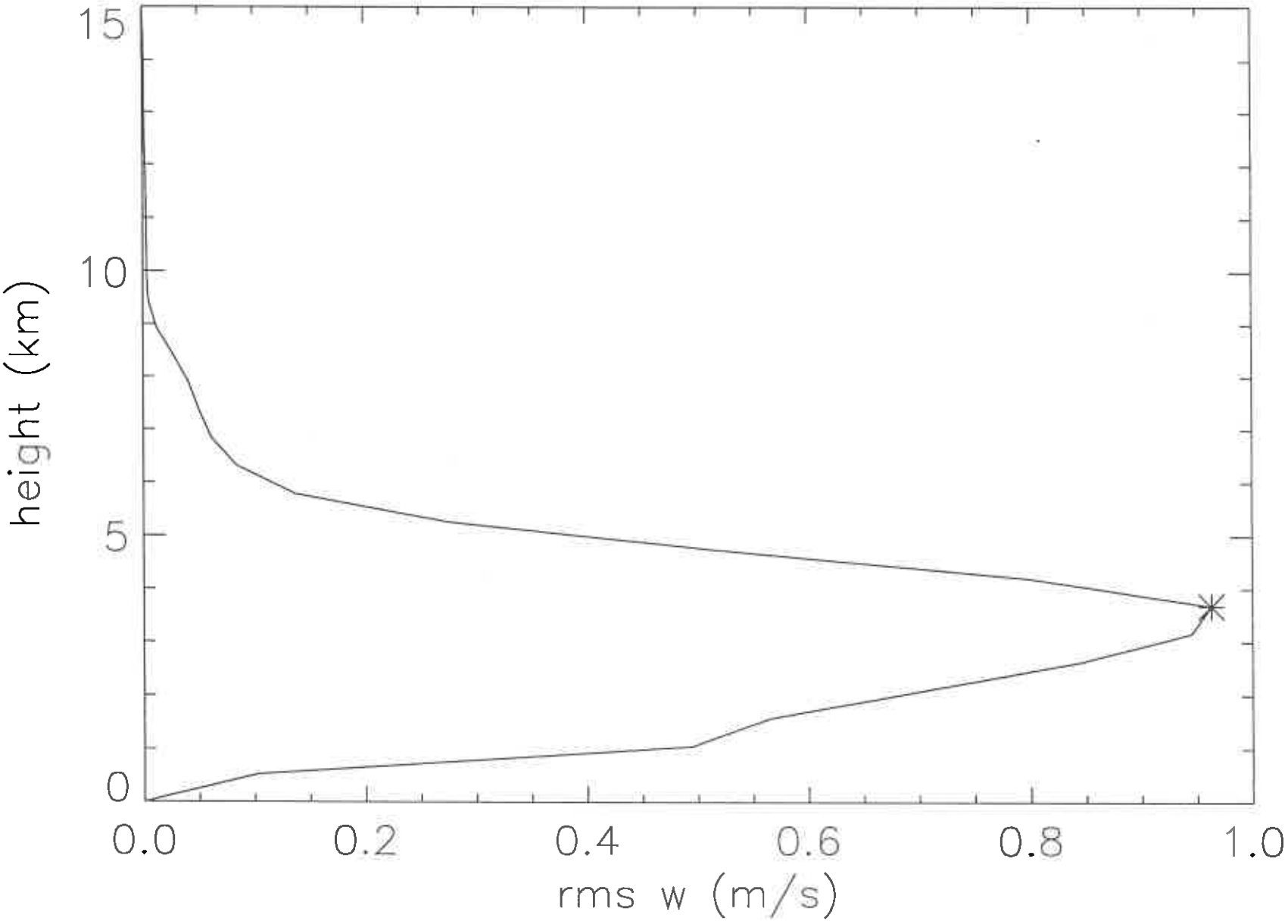

02/11/1995 16:32:17.000

Fig. 5 Vertical profile of momentum flux averaged over second hour of control simulation [180].

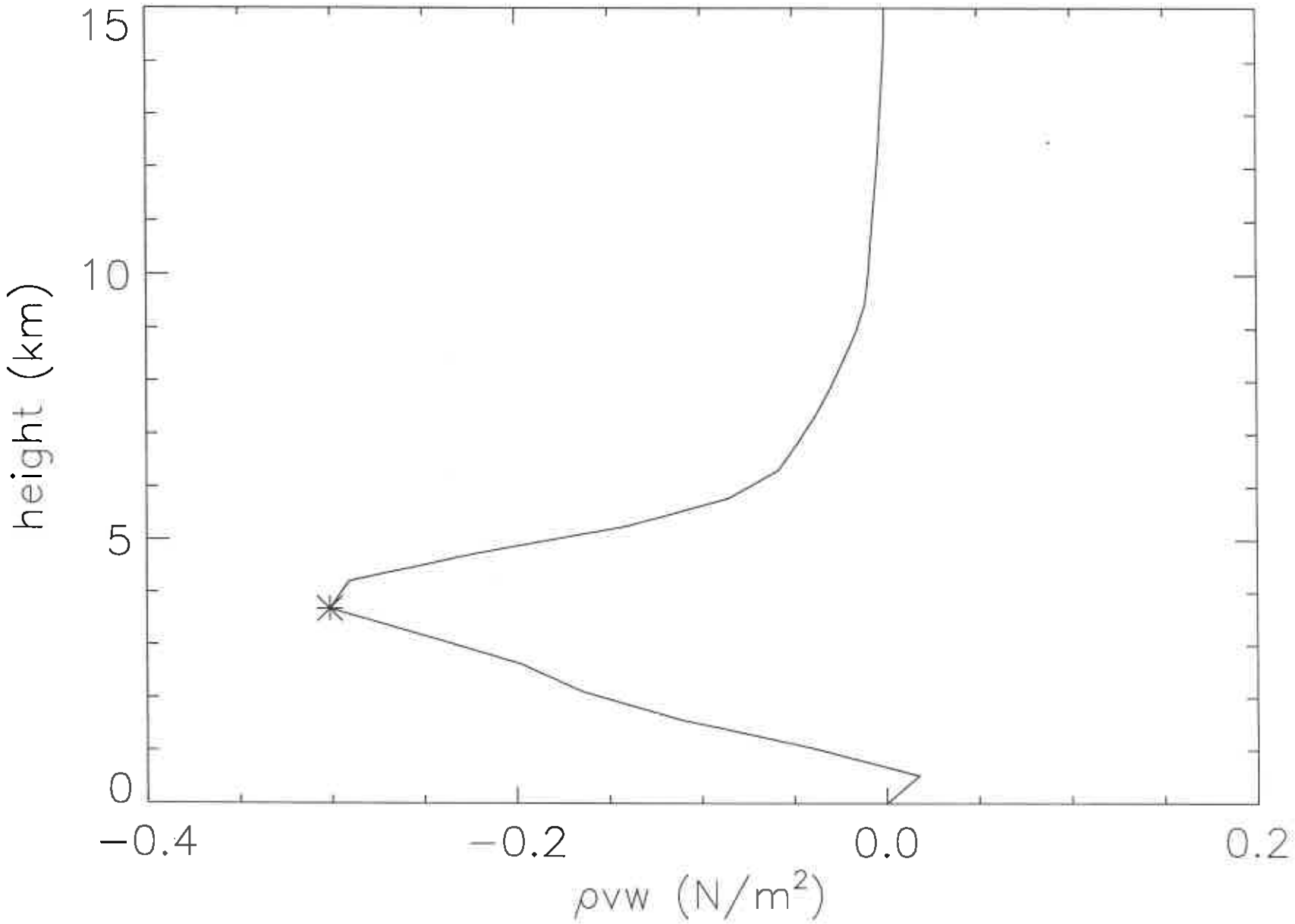

27/10/1995 16:39:58.000

Fig. 6 Scatter plot of momentum flux plotted against product of shear and rms w, averaged over second hour of the numerical experiments.

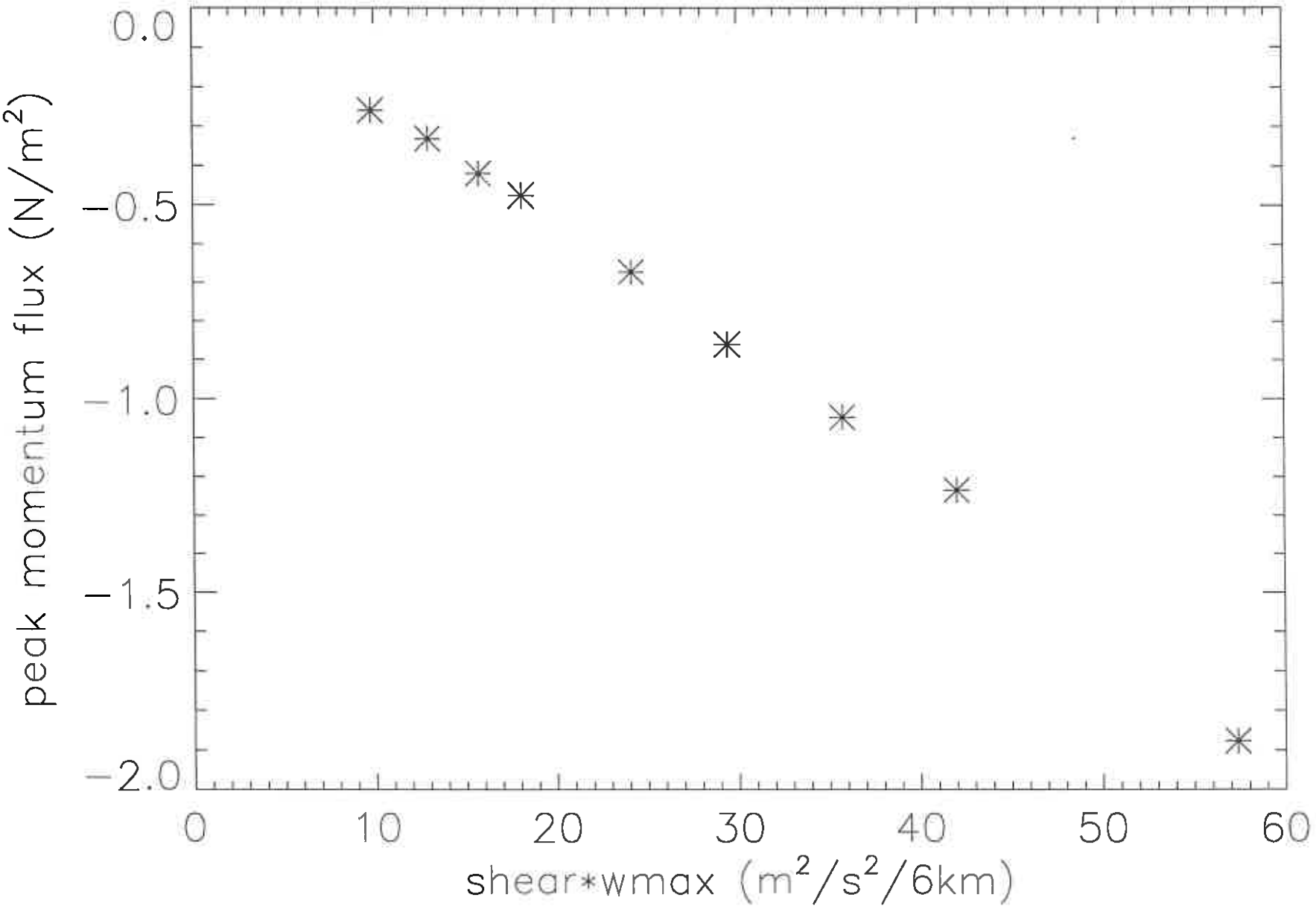

26/10/1995 16:51:04.000

Fig. 7 Vertical profile of partitioned mass fluxes averaged over ten hours of simulations [232] (stars: updraught; diamonds: downdraught) and [236] (squares: updraught; plus signs: downdraught).

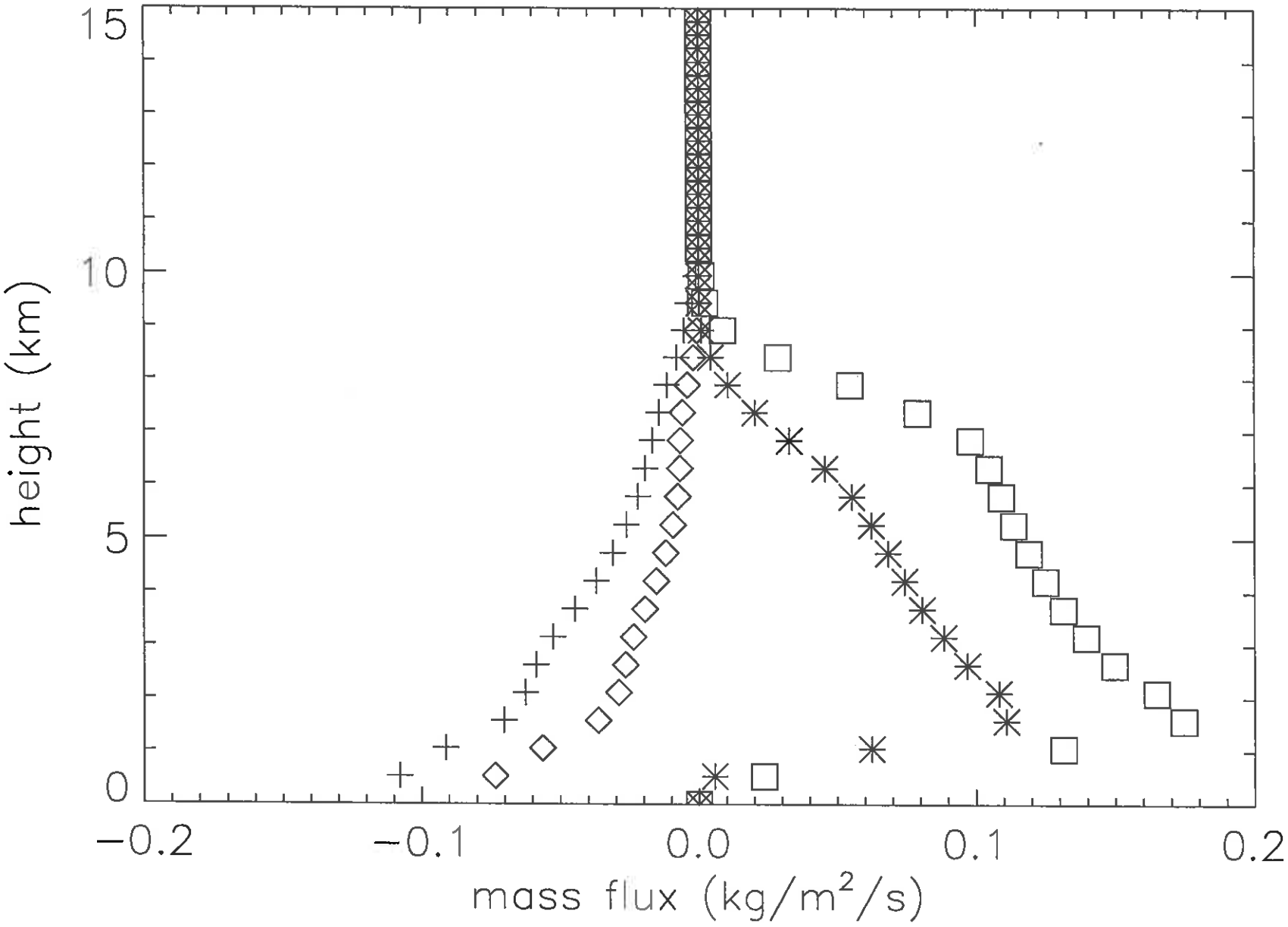

21/11/1995 10:19:36.000

Fig. 8 Vertical profile of acceleration due to horizontal pressure gradient averaged over ten hours of control simulation [232] (stars: updraught; diamonds: downdraught).

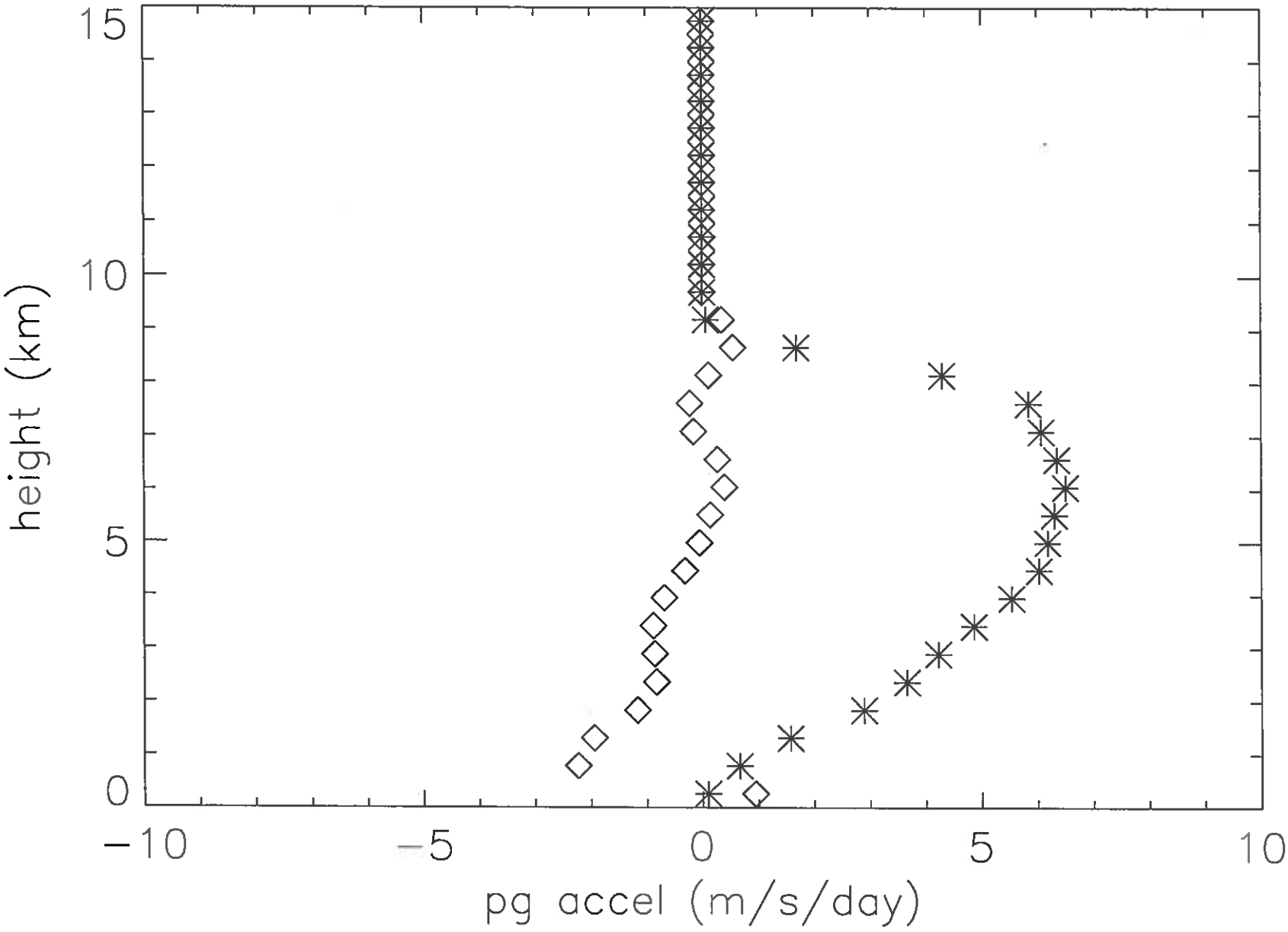

02/11/1995 16:30:12.000

Fig. 9 Vertical profile of partitioned velocities averaged over ten hours of control simulation [232] (solid line: domain average; stars: updraught; diamonds: downdraught).

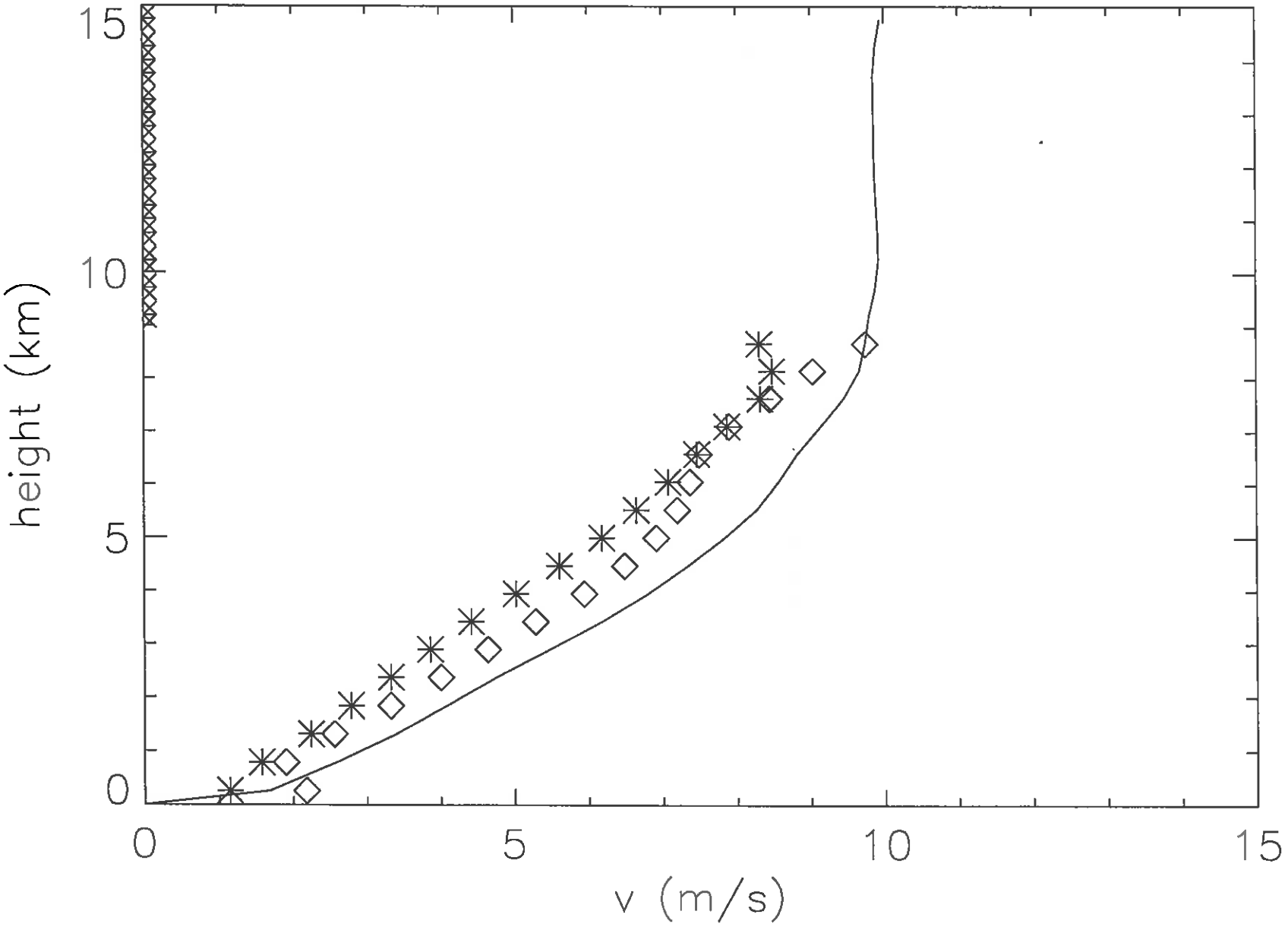

02/11/1995 16:42:36.000

Fig. 10 Vertical profile of partitioned momentum fluxes averaged over ten hours of control simulation [232] (solid line: domain average; stars: updraught; diamonds: downdraught) plus estimates based on equation 7 (dashed: updraught estimate; dash-dotted: downdraught estimate).

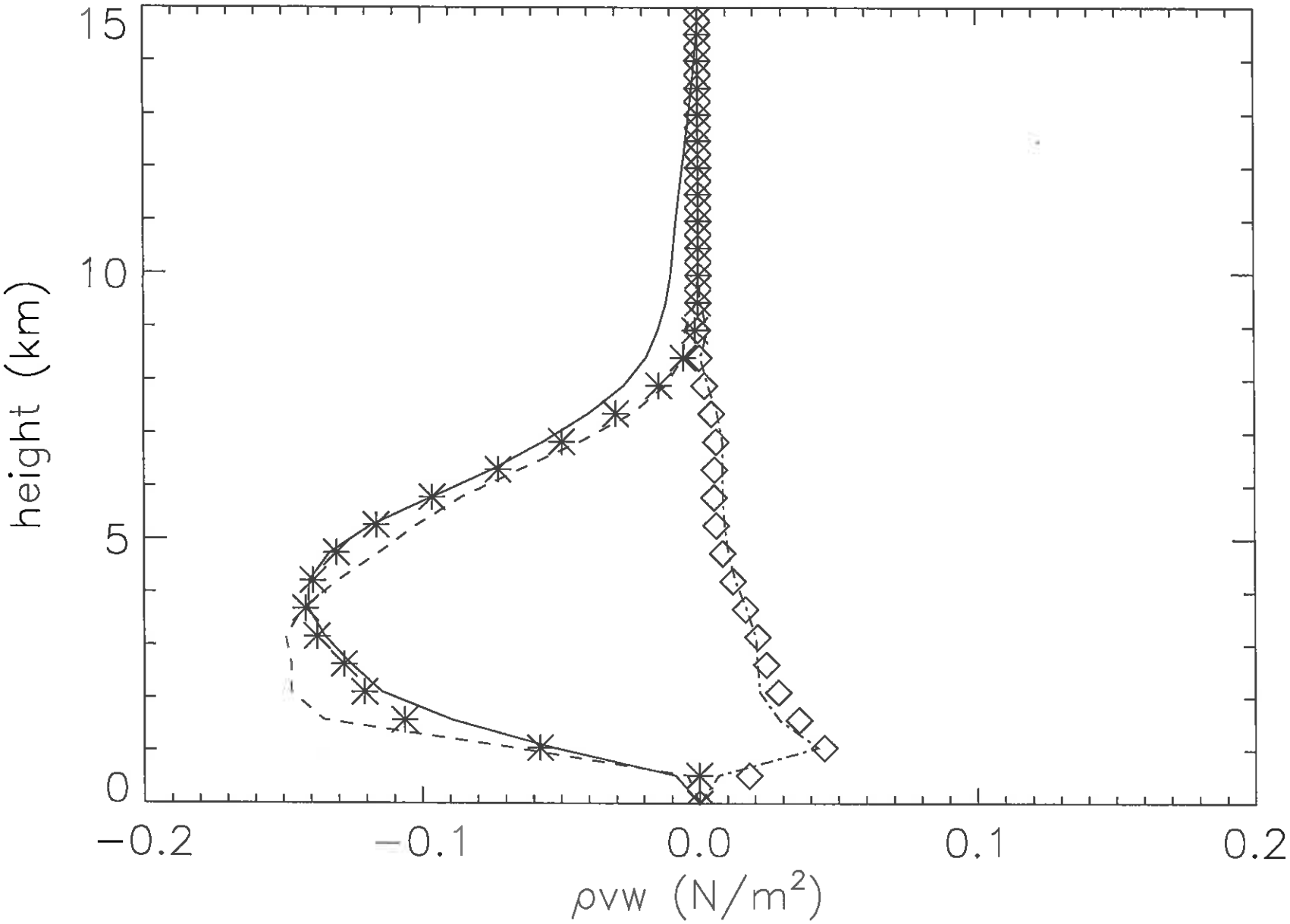

02/11/1995 16:58:26.000

Fig. 11 Change in $\overline{v}$ over ten hours of simulation (plus signs: [232], stars: [233], diamonds: [236], crosses: [237]).

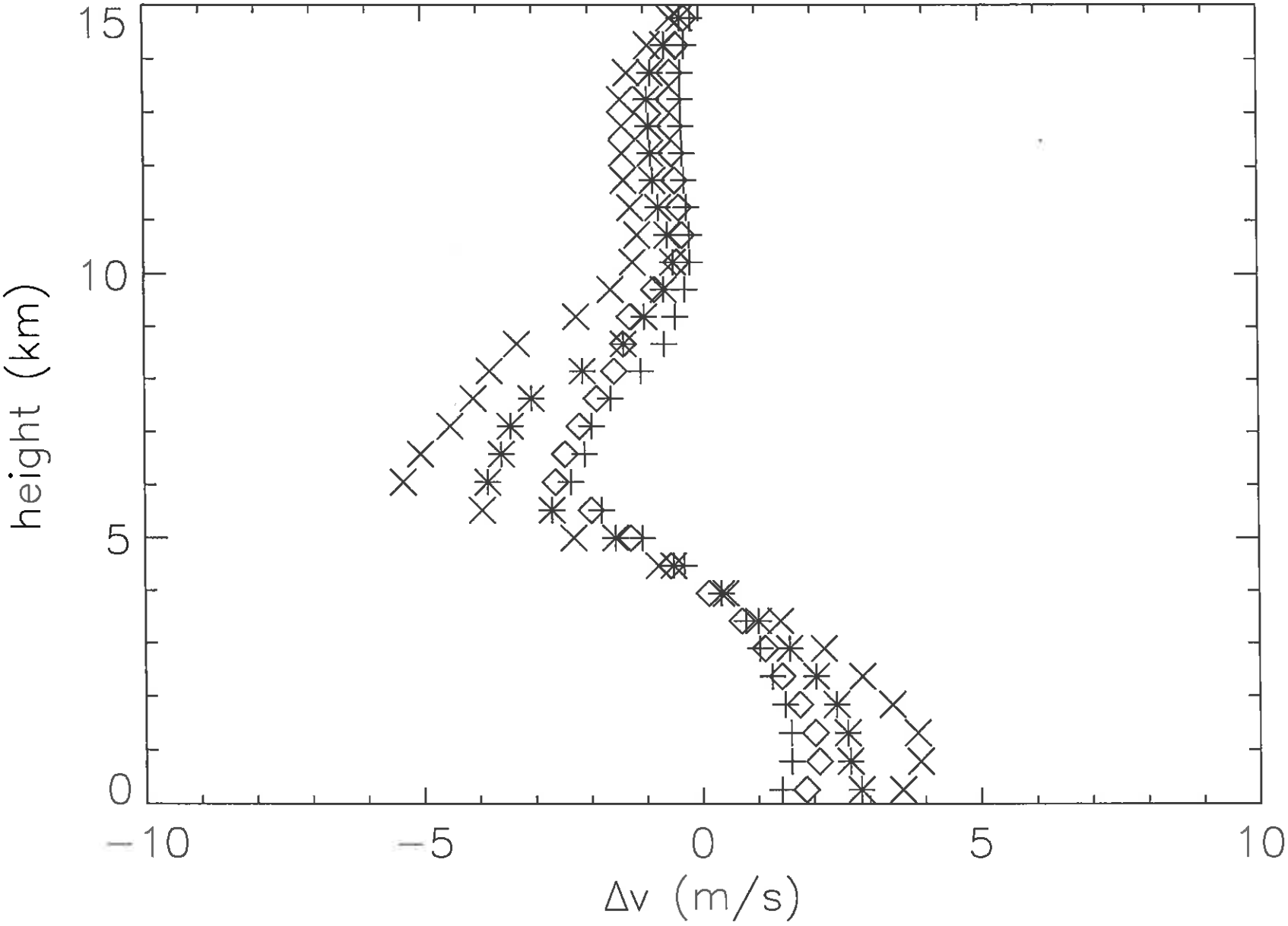

03/11/1995 09:22:21.000

Fig. 12 Change in $\overline{v}$ over ten hours of simulation (plus signs: [237], stars: [242], diamonds: [246], triangles: [247], crosses: [248]).

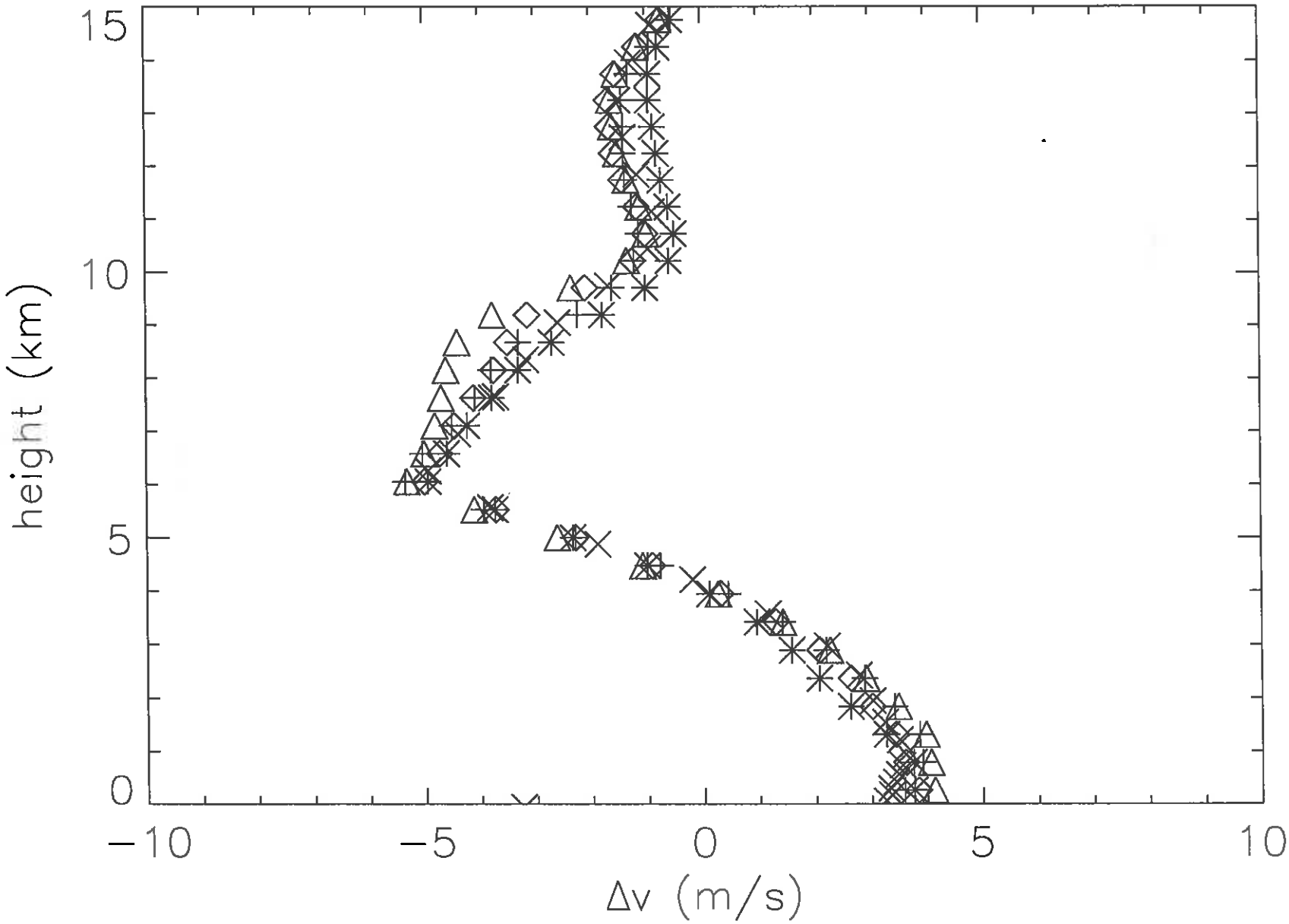

03/11/1995 09:52:35.000

Fig. 13 Initial profiles of (a) θ (solid) and θ_e (stars), (b) q_t (solid) and q_{sat} (crosses), and (c) v in tropical experiments.

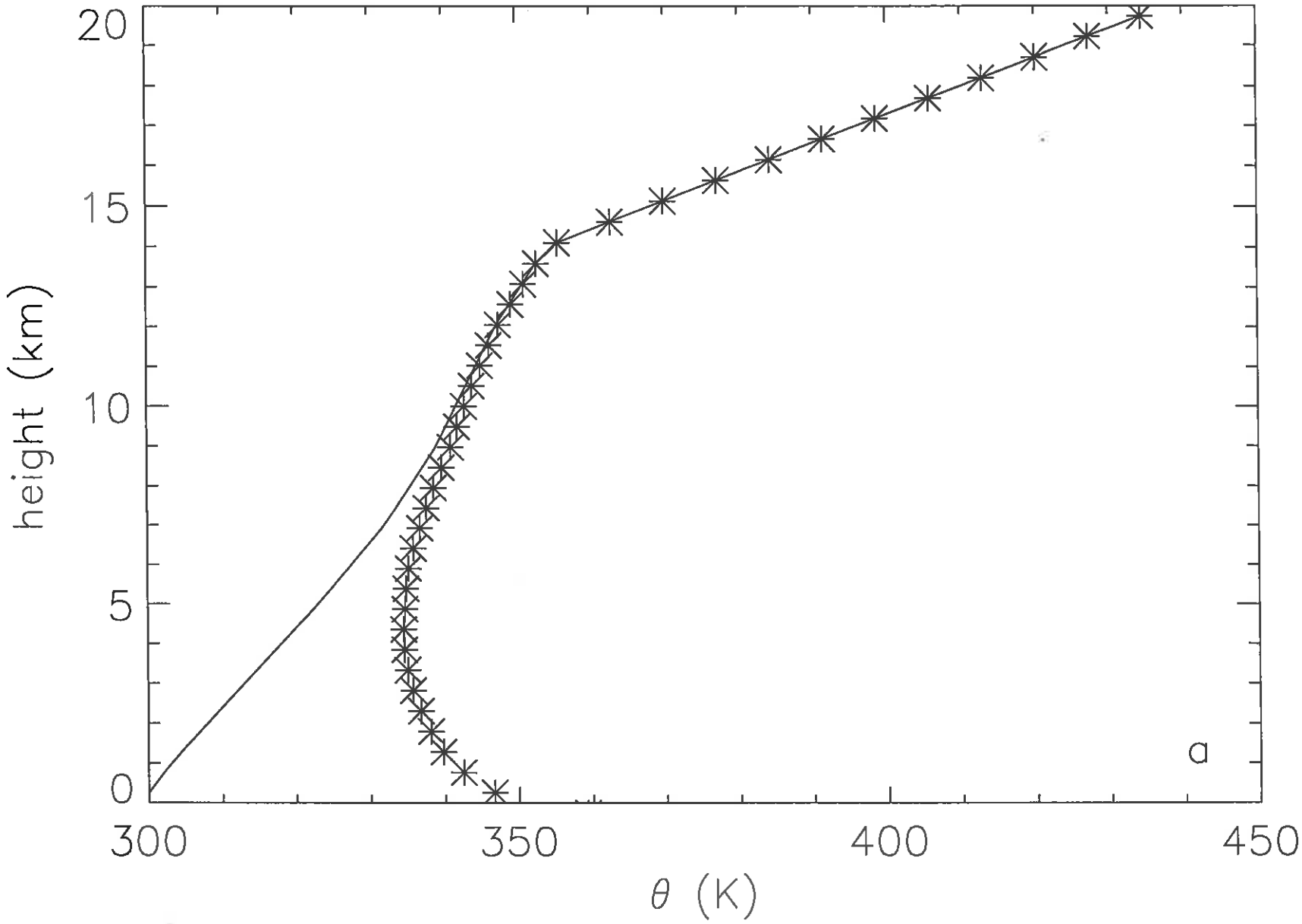

03/11/1995 10:12:18.000

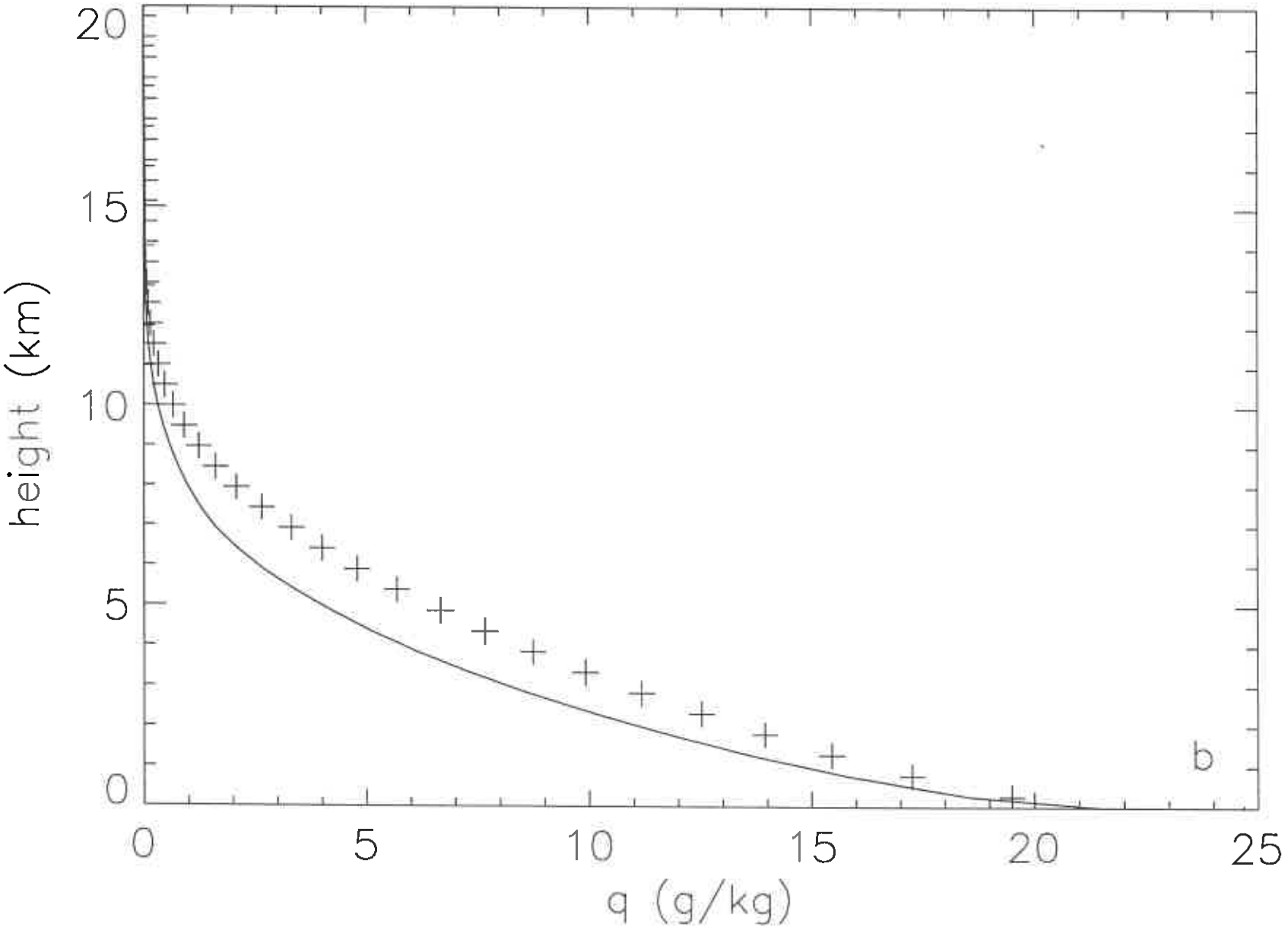

03/11/1995 10:27:02.000

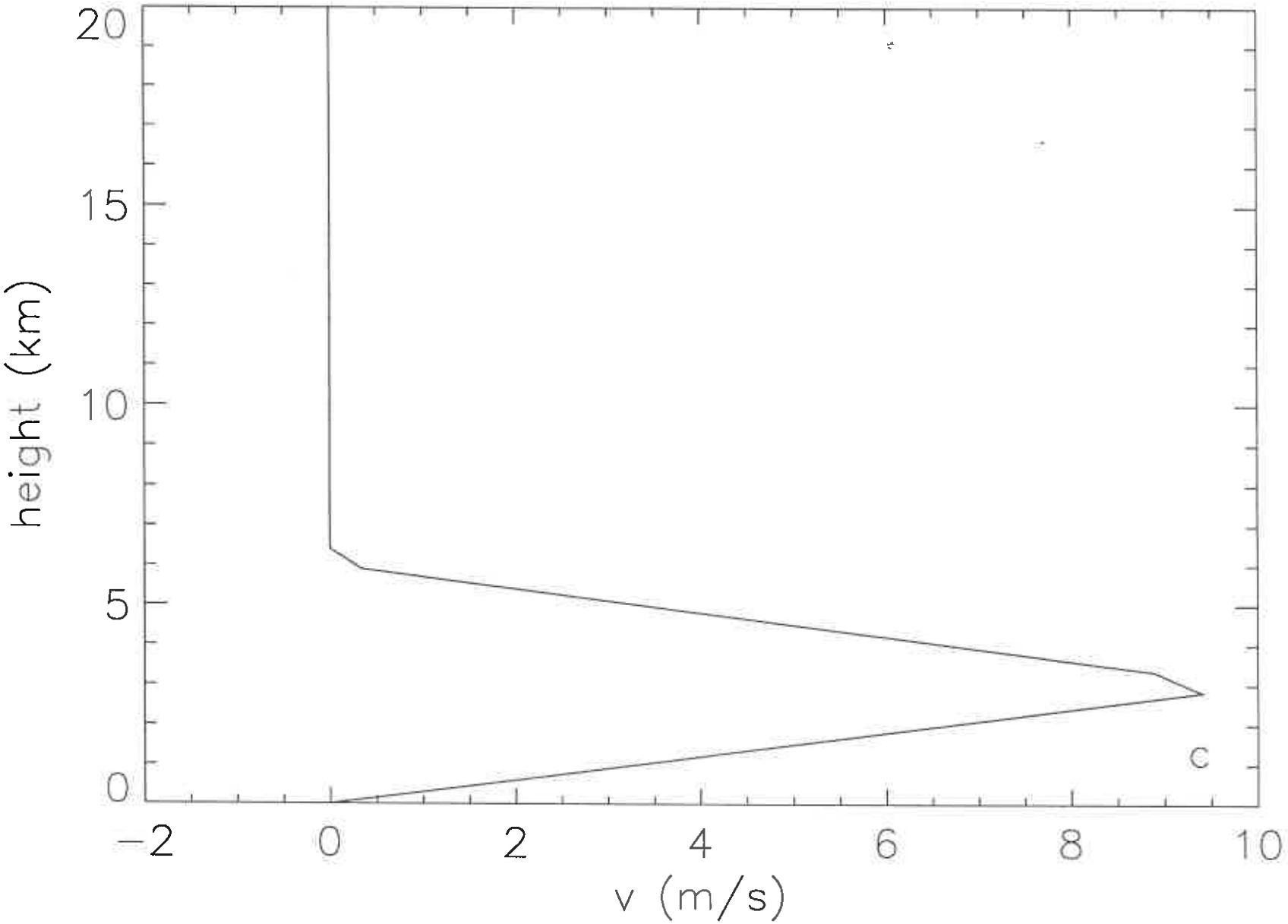

03/11/1995 10:50:07.000

Fig. 14 Forcing profiles for temperature (solid), and moisture (dashed) in tropical experiments.

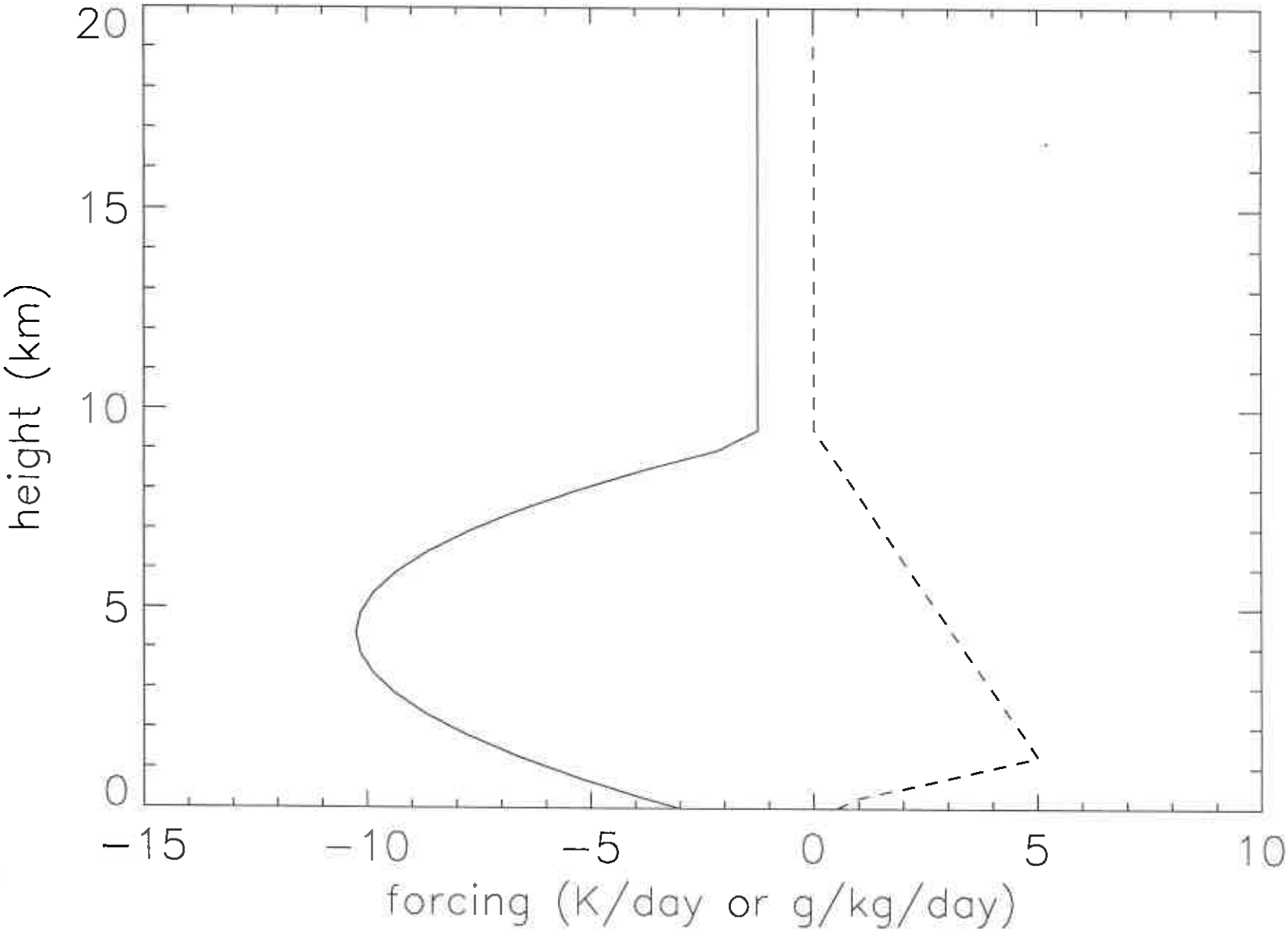

03/11/1995 10:36:34.000

Fig. 15 Vertical profile of partitioned mass fluxes averaged over ten hours of simulations [235] (stars: updraught; diamonds: downdraught) and [234] (plus signs: updraught; triangles: downdraught).

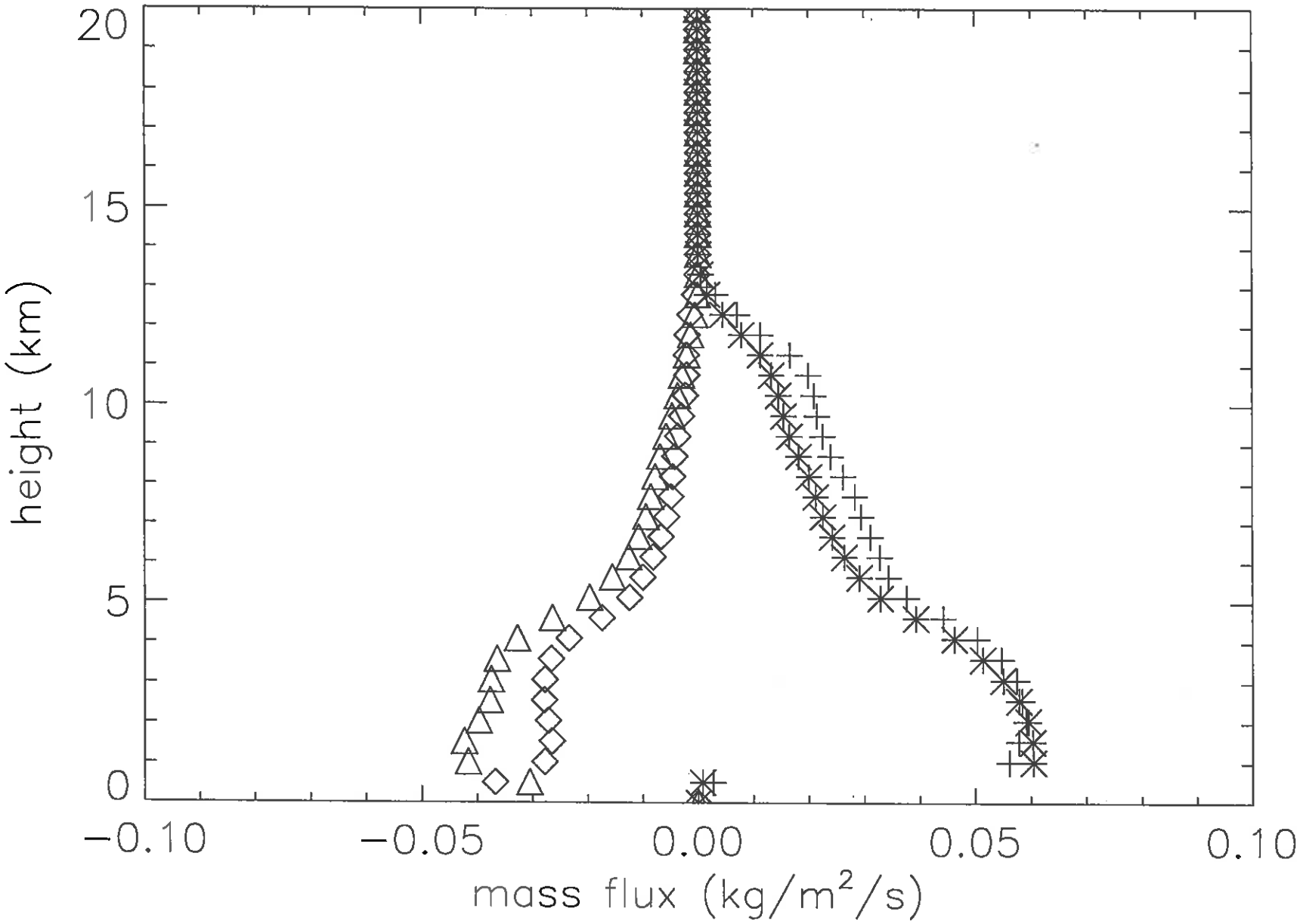

03/11/1995 12:48:25.000

Fig. 16 Vertical profile of acceleration due to horizontal pressure gradient averaged over ten hours of simulation [235] (stars: updraught; diamonds: downdraught).

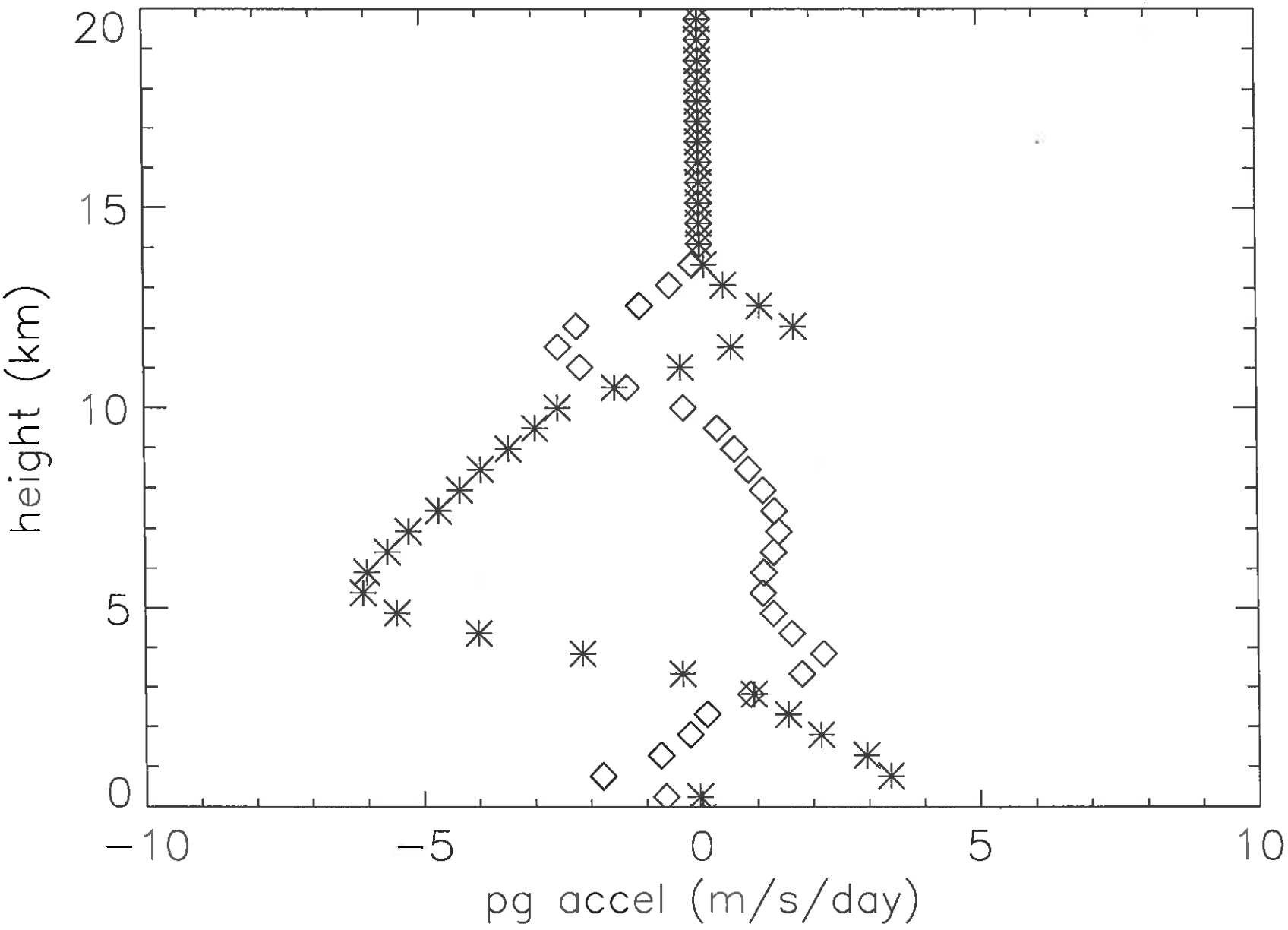

03/11/1995 13:26:41.000

Fig. 17 Vertical profile of partitioned momentum fluxes averaged over ten hours of simulation [235] (solid line: domain average; stars: updraught; diamonds: downdraught) plus estimates based on equation 7 (dashed: updraught estimate; dash-dotted: downdraught estimate).

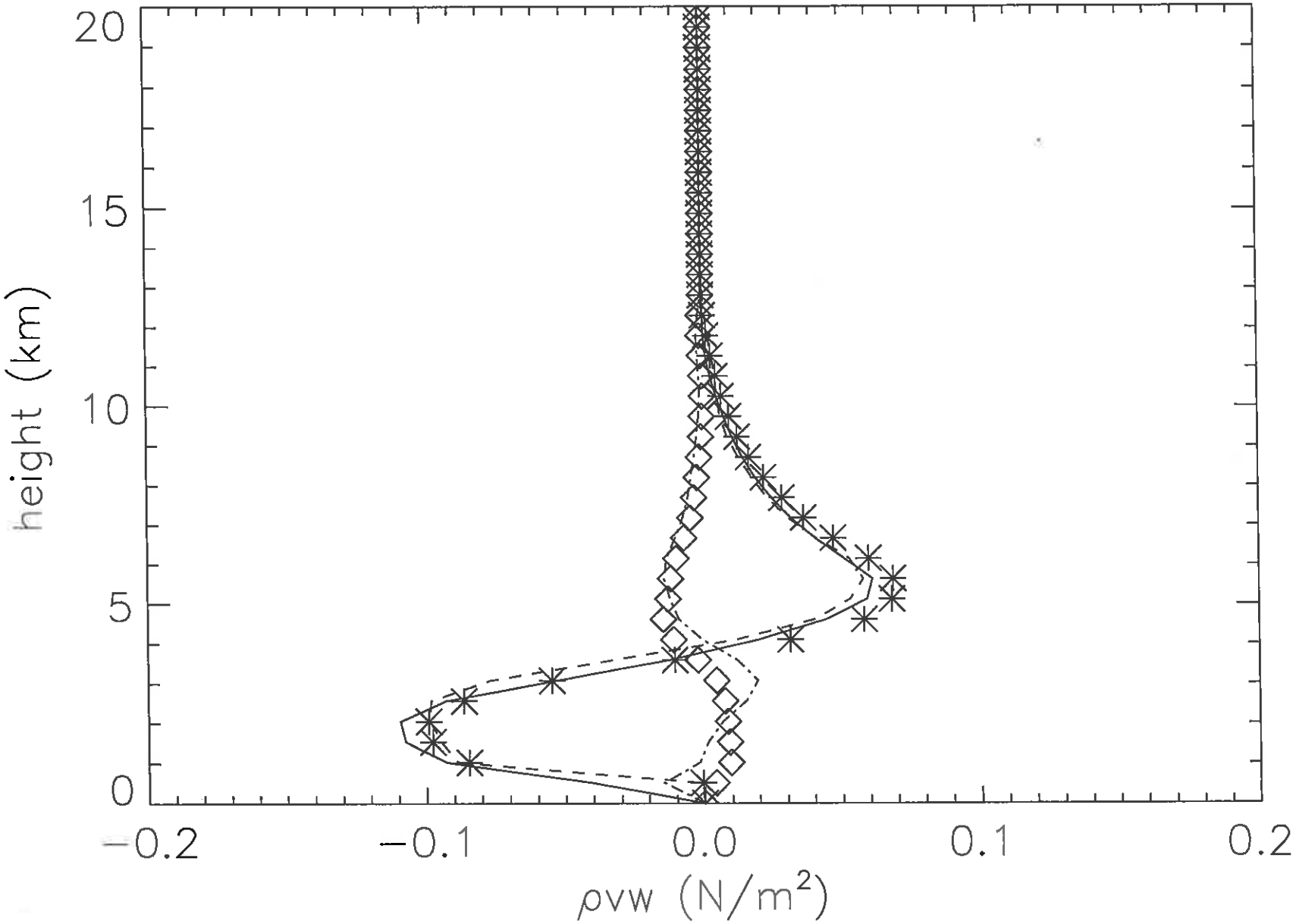

03/11/1995 12:35:49.000

Fig. 18 $\bar{v}$ initially (solid), after ten hours of 3-D simulation [235] (dashed), and after ten hours of 2-D simulation [234] (dotted).

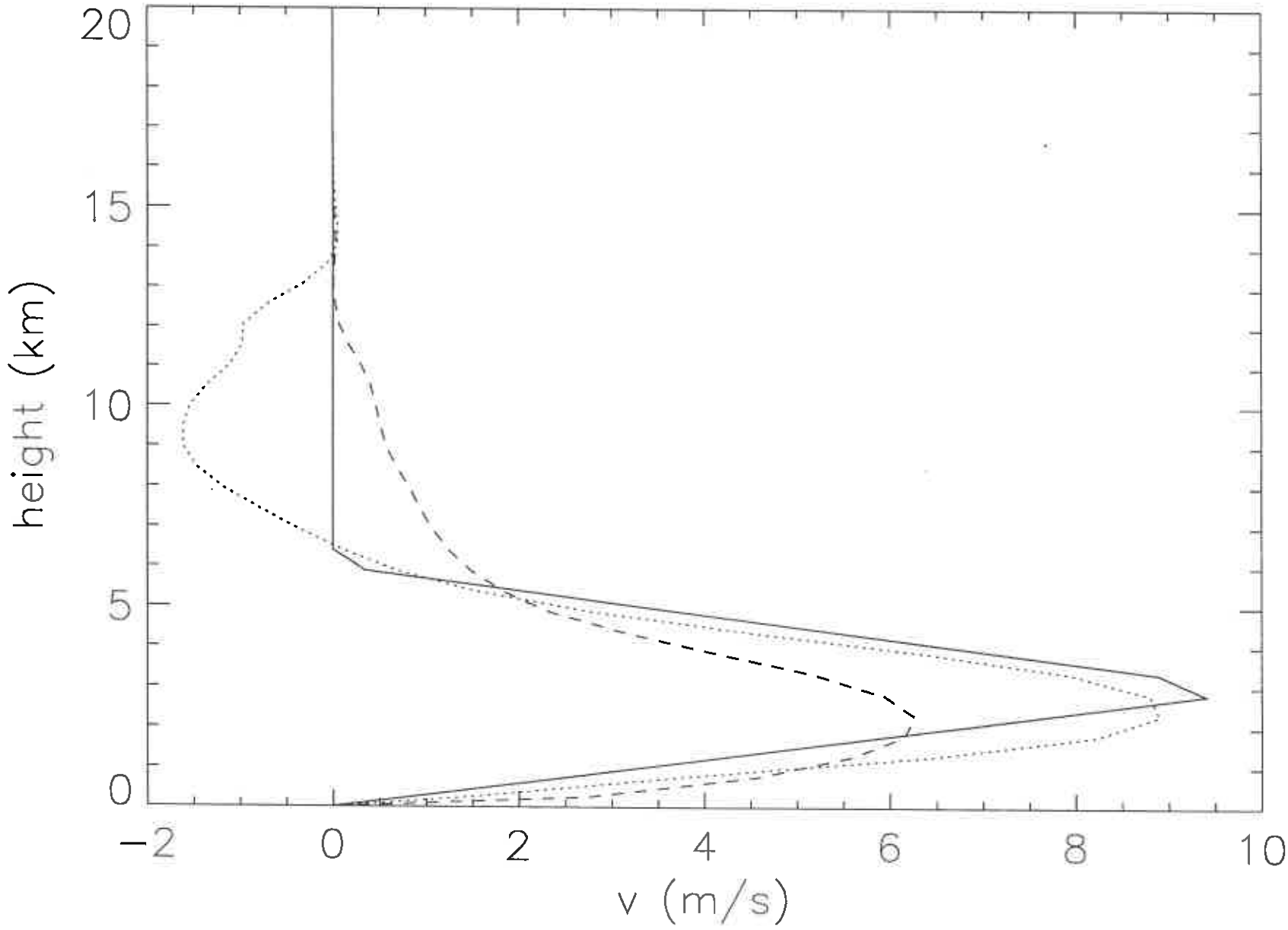

Fig. 19 Vertical profile of acceleration due to horizontal pressure gradient averaged over ten hours of simulation [234] (plus signs: updraught; triangles: downdraught).

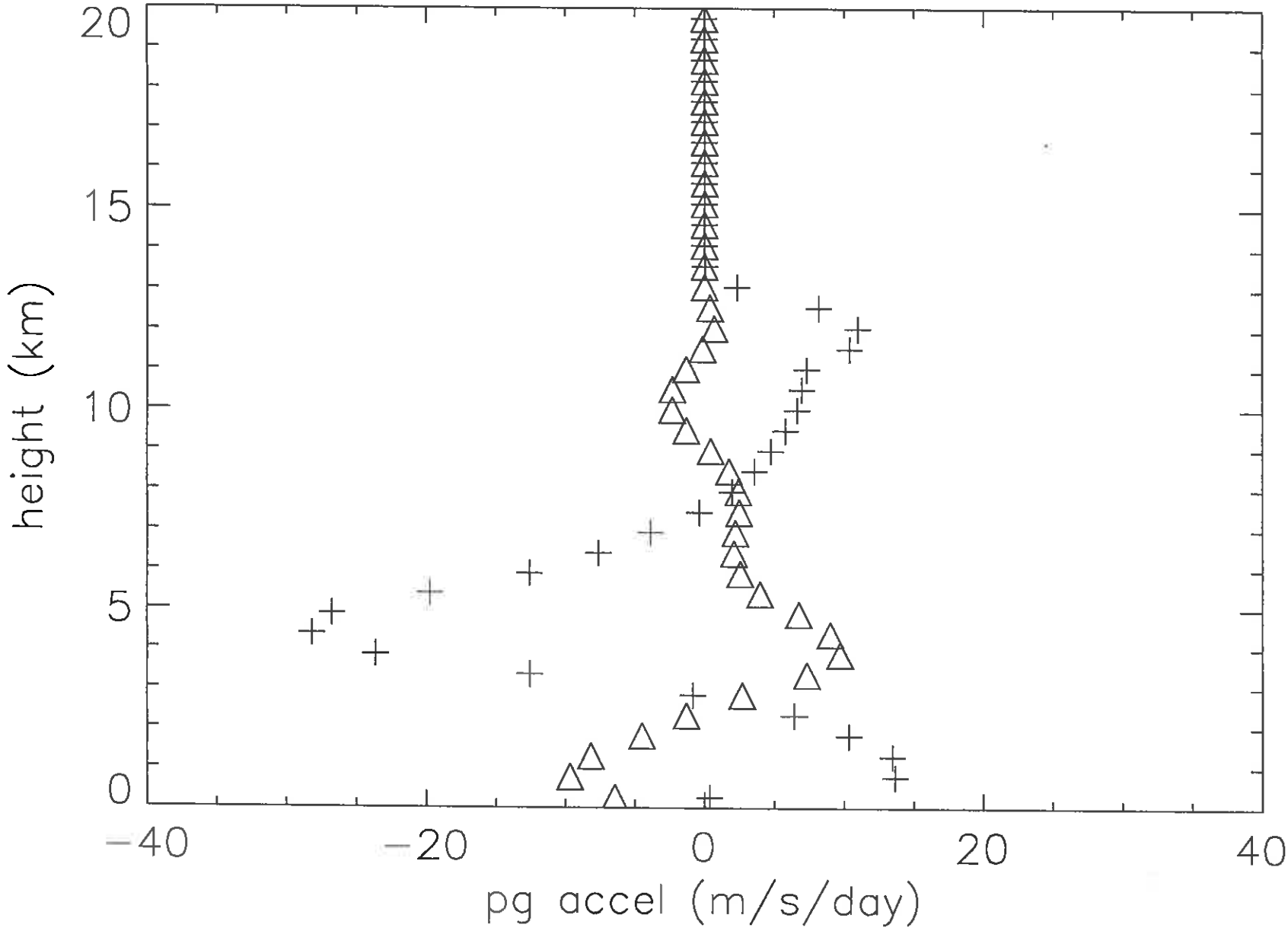

03/11/1995 13:24:42.000

Fig. 20 Vertical profile of partitioned momentum fluxes averaged over ten hours of simulation [234] (solid line: domain average; plus signs: updraught; triangles: downdraught) plus estimates based on equation 7 (dashed: updraught estimate; dash-dotted: downdraught estimate).

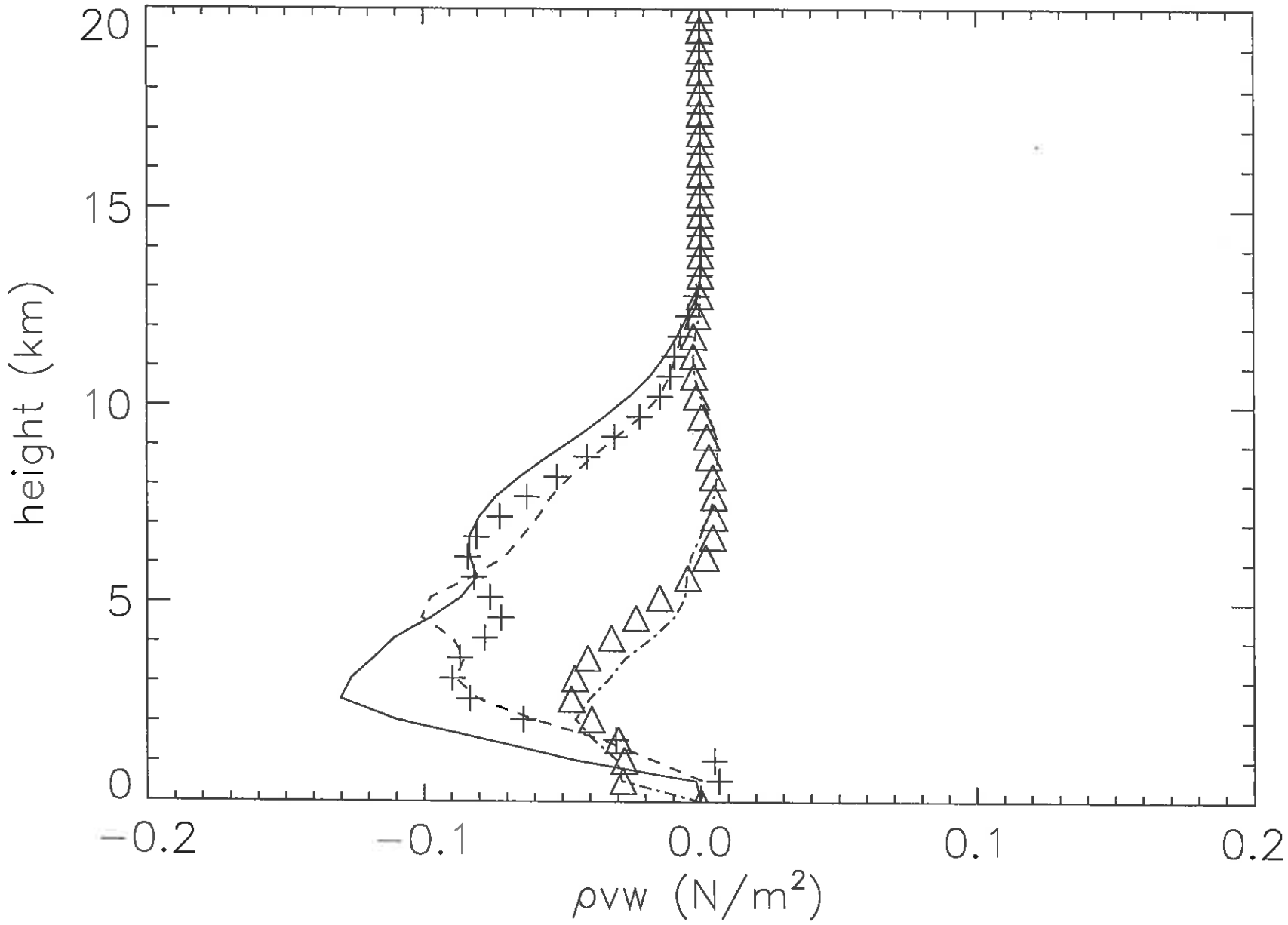

03/11/1995 13:36:27.000

Fig. 21 Vertical section showing wind vectors in part of domain of simulation [234] after 6 hours. The horizontal mean has been subtracted from the v-component.

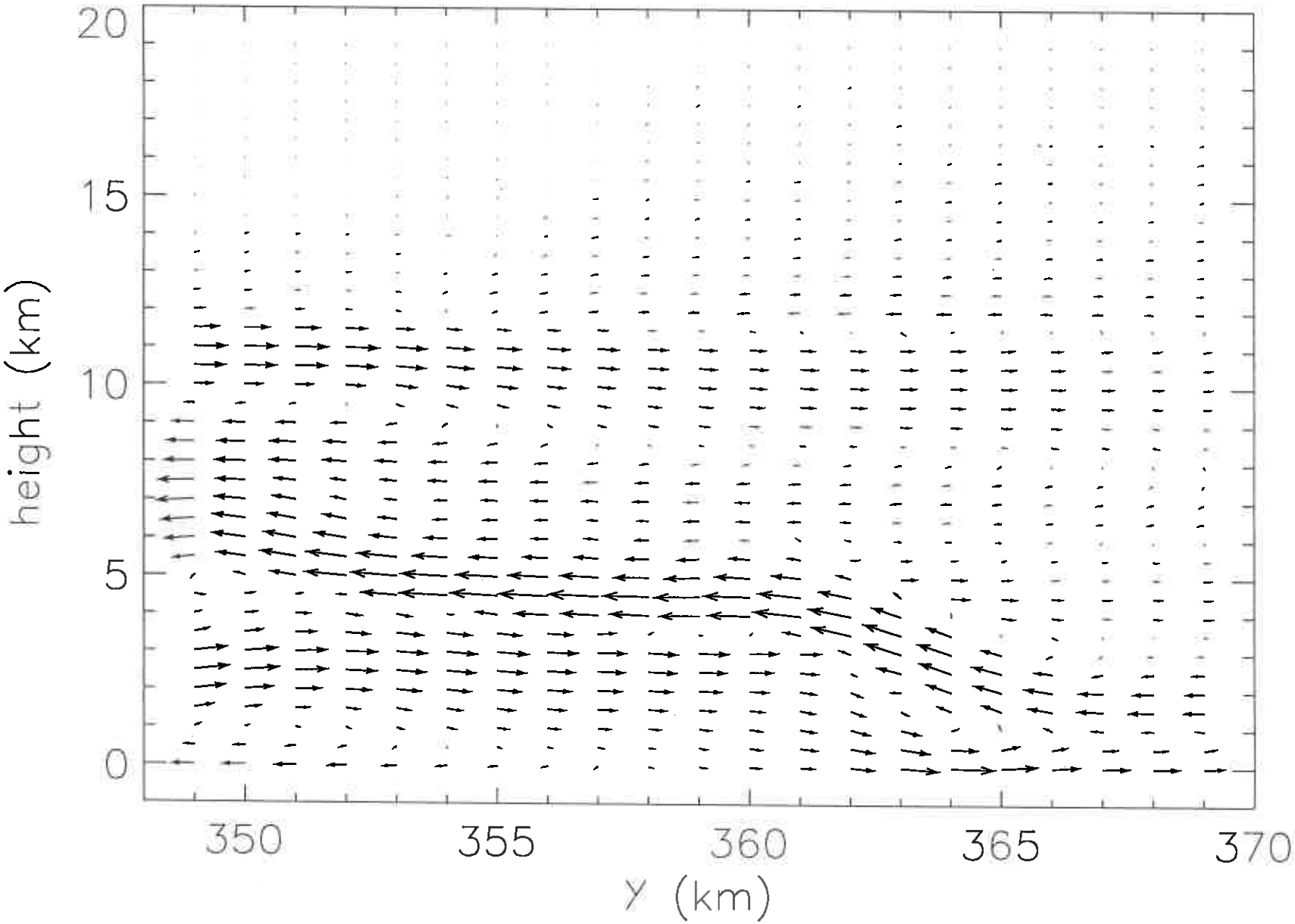

03/11/1995 15:49:56.000

CURRENT JCMM INTERNAL REPORTS

This series of JCMM Internal Reports, initiated in 1993, contains unpublished reports and also versions of articles submitted for publication. The complete set of Internal Reports is available from the National Meteorology Library on loan, if required.

1. **Research Strategy and Programme.**
   K A Browning et al
   January 1993

2. **The GEWEX Cloud System Study (GCSS).**
   GEWEX Cloud System Science Team
   January 1993

3. **Evolution of a mesoscale upper tropospheric vorticity maximum and comma cloud from a cloud-free two-dimensional potential vorticity anomaly.**
   K A Browning
   January 1993

4. **The Global Energy and Water Cycle**
   K A Browning
   July 1993

5. **Structure of a midlatitude cyclone before occlusion.**
   K A Browning and N Roberts
   July 1993

6. **Developments in Systems and Tools for Weather Forecasting.**
   K A Browning and G Szejwach
   July 1993

7. **Diagnostic study of a narrow cold frontal rainband and severe winds associated with a stratospheric intrusion.**
   K A Browning and R Reynolds
   August 1993

8. **Survey of perceived priority issues in the parametrizations of cloud-related processes in GCMs.**
   K A Browning
   September 1993

9. **The Effect of Rain on Longwave Radiation.**
   I Dharssi
   September 1993

10. **Cloud Microphysical Processes - A Description of the Parametrization used in the Large Eddy Model.**
H Swann
July 1994

11. **An Appreciation of the Meteorological Research of Ernst Kleinschmidt.**
A J Thorpe
May 1992

12. **Potential Vorticity of Flow Along the Alps.**
A J Thorpe, H Volkert and Dietrich Heimann
August 1992

13. **The Representation of Fronts.**
A J Thorpe
January 1993

14. **A Parametrization Scheme for Symmetric Instability: Tests for an Idealised Flow.**
C S Chan and A J Thorpe
February 1993

15. **The Fronts 92 Experiment: a Quicklook Atlas.**
Edited by T D Hewson
November 1993

16. **Frontal wave stability during moist deformation frontogenesis. Part 1. Linear wave dynamics**
C H Bishop and A J Thorpe
May 1993

17. **Frontal wave stability during moist deformation frontogenesis. Part 2. The suppression of non-linear wave development.**
C H Bishop and A J Thorpe
May 1993

18. **Gravity waves in sheared ducts.**
S Monserrat and A J Thorpe
October 1993

19. **Potential Vorticity and the Electrostatics Analogy: Quasi-Geostrophic Theory.**
C Bishop and A J Thorpe
November 1993

20. **Recent Advances in the Measurement of Precipitation by Radar.**
A J Illingworth
April 1993

21. **Micro-Physique et Givrage. Cloud Microphysics and Aircraft Icing.**
A J Illingworth
May 1993

22. **Differential Phase Measurements of Precipitation.**
M Blackman and A J Illingworth
May 1993

23. **Estimation of Effective Radius of Cloud Particles from the Radar Reflectivity.**
N I Fox and A J Illingworth
May 1993

24. **A Simple Method of Dopplerising a Pulsed Magnetron Radar.**
L Hua, A J Illingworth and J Eastment
November 1993

25. **Radiation and Polar Lows.**
George C Craig
February 1994

26. **Collected preprints submitted to International Symposium on the Life Cycles of Extratropical Cyclones; Bergen, Norway, 27 June - 1 July 1994**
April 1994

27. **Convective Frontogenesis**
Douglas J Parker and Alan J Thorpe
April 1994

28. **Improved Measurement Of The Ice Water Content In Cirrus Using A Total Water Evaporator**
Philip R A Brown and Peter N Francis
April 1994

29. **Mesoscale Effects of a Dry Intrusion within a Vigorous Cyclone**
K A Browning and B W Golding
April 1994

30. **GEWEX Cloud System Study, Science Plan**
May 1994

31. **Parametrization of Momentum Transport by Convectively Generated Gravity Waves**
R Kershaw
February 1995

32. **Mesoscale Modelling Newsletter, No. 5**
May 1994

33. **Observations of the mesoscale sub-structure in the cold air of a developing frontal cyclone**
K A Browning, S A Clough, C S A Davitt, N M Roberts and T D Hewson
May 1994

34. **Longwave Radiative Forcing of a Simulated Tropical Squall Line**
Imtiaz Dharssi
July 1994

35. **On the nature of the convective circulations at a kata-cold front**
K A Browning
September 1994

36. **Collected preprints of papers submitted to the COST-75 International Seminar on Advanced Weather Radar Systems, Brussels, 20-23 September 1994**
November 1994

37. **Use of satellite imagery to diagnose events leading to frontal thunderstorms: Parts I and II of a case study**
K A Browning and N M Roberts
November 1994

38. **The role of spaceborne millimetre-wave radar in the global monitoring of ice cloud**
P R A Brown, A J Illingworth, A J Heymsfield, G M McFarquhar, K A Browning and M Gosset
December 1994

39. **Potential Vorticity Inversion**
Michal Ziemianski
October 1994

40. **Theory of mature tropical cyclones; A comparison between Kleinschmidt (1951) and Emanual (1986)**
Suzanne L Gray
December 1994

41. **Dispersion and removal of pollutants during the passage of an atmospheric frontal system**
N R Gimson
December 1994

42. **The role of snow sublimation in frontogenesis**
D J Parker and A J Thorpe
December 1994

43. **Potential vorticity and the electrostatics Analogy: Ertel-Rossby formulation**
A J Thorpe and C H Bishop
December 1994

44. **Mesoscale aspects of extratropical cyclones: an observational perspective**
K A Browning
January 1995

45. **A Polar Low Outbreak: Evolution and Mesoscale Structures**
T D Hewson, G C Craig and C Claud
February 1995

46. **Generation of near-surface gusts by deep convection**
K Nakamura and R Kershaw
April 1995

47. **Attribution concepts applied to the omega equation**
S A Clough, C S A Davitt and A J Thorpe
June 1995

48 **Parametrization of mixed-phase cloud and precipitation**
Susan P Ballard and M Gerard Hutchinson
June 1995

49 **Short-range forecasting of stratocumulus: Initialization V Prediction**
Susan P Ballard, Simon D Jackson and B Macpherson
June 1995

50 **Contributions of the JCMM/Dept of Meteorology Radar Group to the 27th AMS Radar Meteorology Conference, Vail October 1995**
June 1995

51 **Cold pools in shear**
Douglas J Parker
September 1995

52 **High-resolution analysis of frontal fracture**
K A Browning, S P Ballard and C S A Davitt
September 1995

53 **The Albedo of Broken Cloud Fields: Calculations using a modified two stream radiation code**
Imtiaz Dharssi and Roy Kershaw
October 1995

54 **Parametrization of momentum transport by convection. I: Theory and cloud modelling results**
R Kershaw and D Gregory
November 1995

Met Office Joint Centre for Mesoscale Meteorology Department of Meteorology
University of Reading PO Box 243 Reading RG6 6BB United Kingdom
Tel: +44 (0)118 931 8425 Fax: +44 (0)118 931 8791
www.metoffice.com